https://doi.org/10.5194/egusphere-2022-696
Preprint. Discussion started: 18 October 2022

Surface snow bromide and nitrate at Eureka, Canada in early spring and implications for polar boundary layer chemistry

Xin Yang[1], Kimberly Strong[2], Alison S. Criscitiello[3], Marta Santos-Garcia[1*], Kristof Bognar[2**], Xiaoyi Zhao[4], Pierre Fogal[2], Kaley A. Walker[2], Sara M., Morris[5], and Peter Effertz[6,7]

[1]British Antarctic Survey, Natural Environment Research Council, Cambridge, UK
[2]Department of Physics, University of Toronto, Toronto, ON, Canada
[3]Department of Earth and Atmospheric Sciences, University of Alberta, Edmonton, Alberta, Canada
[4]Air Quality Research Division, Environment and Climate Change Canada, Toronto, ON, Canada
[5]NOAA Earth System Research Laboratories, Physical Sciences Laboratory, Boulder, CO, USA
[6]Cooperative Institute for Research in Environmental Science - CU Boulder, Boulder, CO, USA
[7]NOAA Earth System Research Laboratories, Global Monitoring Laboratory, Boulder, CO, USA

[*]Now at School of Geosciences, University of Edinburgh, Edinburgh, UK

[**]Now at 3v Geomatics Inc., Vancouver, BC, Canada

Correspondence to: Xin Yang (xinyang55@bas.ac.uk)

Abstract. This study explores the role of snowpack in polar boundary layer chemistry, especially as a direct source of reactive bromine (BrO_X=BrO+Br) and nitrogen (NO_X=NO+NO_2) in the Arctic springtime. Surface snow samples were collected daily from a Canadian high Arctic location at Eureka, Nunavut (80°N, 86°W) from the end of February to the end of March in 2018 and 2019. The snow was sampled at several sites representing distinct environments: sea ice, inland close to sea level, and a hilltop ~600 m above sea level (asl).

At the inland sites, surface snow salinity has a double-peak distribution with the first and lowest peak at 0.001-0.002 practical salinity unit (psu), which corresponds to the precipitation effect, and the second peak at 0.01–0.04 psu, likely due to the condensation effect. Snow salinity on sea ice has a triple-peak distribution; its first and second peaks overlap with the inland peaks, and the third peak at 0.2–0.4 psu can be clearly attributed to sea water contamination.

At all sites, sodium and chloride concentrations in surface snow increase by almost 10-fold from the top 0.2 cm to ~1 cm in depth. Bromide in surface snow is significantly enriched, indicating that surface snow at Eureka is a net sink of atmospheric bromine. Moreover, daily data show that top surface snow bromide at all sampling sites has an increasing trend over the measurement time period (late February to late March), with mean slopes of 1.9 and 1.3 ppb d^{-1} in the 0-0.2 cm and the 0.2–0.5 cm layers, respectively. At the sea level sites, snow nitrate also shows a significant increasing trend, with mean slopes of 12.1, 12.4, and 4.3 ppb d^{-1} in the top 0.2 cm, 0.2–0.5 cm, and 0.5–1.5 cm layers, respectively. Using these trends, we derive a novel method to calculate deposition flux of bromide and nitrate to the snowpack. For bromide, the integrated deposition flux is 1.29×10^7 molecules cm^{-2} s^{-1} at sea level and 1.01×10^7 molecules cm^{-2} s^{-1} at ~600 m. For nitrate, the integrated deposition

https://doi.org/10.5194/egusphere-2022-696
Preprint. Discussion started: 18 October 2022

flux is 2.4×10^8 molecules cm^{-2} s^{-1} at sea level and -1.0×10^8 molecules cm^{-2} s^{-1} at ~600 m; the negative flux indicates that snow at the hilltop sites is losing nitrate. The smaller vertical gradient of bromide deposition flux strongly indicates that local snowpack emission on sea ice and inland is not likely to be a large source of reactive bromine. In contrast, nitrate deposition flux has a large vertical gradient, e.g., with a positive flux at sea level and a negative flux at ~600 m, indicating that snowpack at sea level is a large source of reactive nitrate.

In addition, we found a significant correlation (with coefficient R values of 0.48-0.76) between surface snow nitrate and bromide at the inland sites. The $[NO_3^-]/[Br^-]$ ratio ranges from 4 to 7, highlighting the effect of reactive bromine in accelerating the atmospheric NO_X-to-nitrate conversion. This is the first time we see such an effect over the course of one day.

1 Introduction

Reactive bromine (BrO_X=BrO+Br) and reactive nitrogen (NO_X=NO+NO_2) are two important families in atmospheric chemistry, both of which play a critical role in determining the oxidising capacity of the polar boundary layer (Morin et al., 2008). However, the processes involved in the sources, sinks, and recycling of reactive bromine and nitrogen in the air-snow-sea ice system are not fully understood (Abbatt et al., 2012) or parameterised, which prevents quantification of their effects and the ability to make robust predictions for the changing climate using numerical chemical models.

Reactive nitrogen-rich air observed in the Arctic troposphere is mainly anthropogenic and subject to long-range transport (Dickerson, 1985). During winter, gaseous nitric acid (HNO_3) or particulate bond nitrate (p-NO_3) is removed from the air via dry and wet deposition. HNO_3 and p-NO_3 mainly dissolve to form nitrate (NO_3^-) upon contact with the snow cover (Diehl et al., 1995; Abbatt, 1997). Nitrate that accumulates in snowpack can release gaseous NO_X and HONO in spring via photolysis (Dubowski et al., 2001; Honrath et al., 2002), with the processes controlled by many factors including meteorological parameters and chemical, optical, and physical snow properties. These include photolabile NO_3^- concentrations, the amount of light-absorbing impurities, the temperature-dependent quantum yields of NO_3^- photolysis, and the timing of precipitation (Beine et al., 2003; Frey et al., 2013; Chan et al., 2015; Zatko et al., 2016; Winton et al., 2020). The measured snow-NO_X emission fluxes in polar regions vary from site to site, ranging from near zero to $>1.0\times10^9$ molecules cm^{-2} s^{-1} (Jones et al., 2001; Zhou et al., 2001; Honrath et al., 2002; Beine et al., 2002; 2003; Oncley et al., 2004; Frey et al., 2013; Chan et l., 2018). A direct measurement of nitrate dry deposition flux was made by Björkman et al. (2013) in Svalbard using a tray sampling approach. They reported a total flux of 10.27±3.84 mg m^{-2} (September 2009 to May 2010) which is roughly equivalent to a mean flux of 4×10^8 molecules cm^{-2} s^{-1}. In addition, precipitation at Svalbard dominates nitrate supply to snow, with dry deposited HNO_3 only accounting for 10-14% of total nitrate (Beine et al., 2003; Björkman et al., 2013).

Observations show that sea-ice regions have the highest tropospheric bromine oxide (BrO) loading on Earth (Wagner and Platt, 1998). BrO enhancements are normally observed in the polar boundary layer during springtime and are referred to as "bromine explosion" events (BEEs). It is well known that saline substrates are the eventual source of reactive bromine (Wagner and Platt, 1998; Oum et al., 1998; Simpson et al., 2007a). However, the dominant sources and the underlying processes

https://doi.org/10.5194/egusphere-2022-696
Preprint. Discussion started: 18 October 2022

involved remain unclear, with more than half a dozen different candidates proposed. These include frost flowers (Kaleschke et al., 2004; Piot and von Glasow, 2008), first-year sea ice surface (Simpson et al., 2005; 2007b), open leads/polynyas (e.g., Peterson et al., 2016; Kirpes et al., 2019; Criscitiello et al., 2021), snowpack on tundra (Pratt et al., 2013), snowpack on sea ice (Custard et al., 2017; Peterson et al., 2019), snowpack on ice sheets (Thomas et al., 2011), and sea salt aerosols from blowing snow (Yang et al., 2008; 2010; 2019, 2020; Frey et al., 2020; Huang et al., 2020). Significant progress has been made in recent decades, with data showing that frost flowers and open leads are only of minor or local importance (Domine et al., 2005; Obbard et al., 2009; Huang et al., 2020). In addition, the proposed stratospheric BrO intrusion (Salawitch et al., 2010) has also been found to be less important than previously thought (Theys et al., 2011). Currently, the major debate surrounds the relative importance of the two remaining candidates – snowpack and blowing snow (e.g., Bognar et al., 2020; Marelle et al., 2021; Swanson et al., 2022).

Reactive bromine can directly cause polar boundary layer ozone depletion events (ODEs), whereby near-surface ozone concentrations in spring drop below 10 ppbv (part per billion by volume), reaching close to 0 ppbv in some cases (Bottenheim et al., 1986; Barrie et al., 1988; Tarasick and Bottenheim, 2002). In addition, BrO_X can affect reactive nitrogen (Morin et al., 2008) and hydroxyl radicals (HO_X=OH+ HO_2) (Bloss et al., 2007, 2010; Brough et al., 2019) as well as elemental mercury oxidation (e.g., Holmes et al., 2006; Parella et al., 2012; Angot et al., 2016; Wang et al., 2019) and dimethyl sulphide oxidation (Hoffmann et al., 2016).

It is well-known that BrO_X can directly react with NO_X via the following reactions:

$$BrO(g) + NO_2(g) \rightarrow BrONO_2(g) \quad (R1)$$

$$BrONO_2(g) + H_2O(aq) \rightarrow HNO_3(g) + HOBr(g) \quad (R2)$$

Thus, the presence of BrO_X may accelerate the conversion from NOx to nitrate and influence the atmospheric nitrogen budget. Previous modelling work has estimated that bromine chemistry can cause NO_X reductions of 60-80% at high latitudes in spring (Yang et al., 2005).

The emission fluxes of reactive bromine from blowing snow are all based on parameterisation in models (Yang et al., 2008; 2010, 2020; Huang et al., 2020; Swanson et al., 2020; Marelle et al., 2021). There are currently no direct measurements of bromine emission flux from blowing snow. Regarding snowpack bromine emission, a direct gradient measurement of Br_2 and BrCl above a patch of snowpack was made near Utqiaġvik, Alaska (Custard et al., 2017), who reported emission fluxes of 0.7–12 × 10^8 molecules cm^{-2} s^{-1}. However, the emission fluxes were based on a field dataset obtained over only a few days. Snowpack parameterisation schemes estimated bromine emission fluxes of 9.0 × 10^7 to 2.7 × 10^9 molecules cm^{-2} s^{-1}, however, the emission flux is highly dependent on the parameters applied (Lehrer et al., 2004; Poit et al., 2009; Toyota et al., 2014; Falk and Sinnhuber, 2018; Marelle et al., 2021). So far, there have not been any direct in-situ measurement of bromine deposition flux to snowpack. The removal of inorganic species (such as HBr, HOBr, Br_2, BrCl, $BrONO_2$ and BrO) from the atmosphere via wet and dry depositions are mainly calculated by models (e.g., Yang et al., 2005; 2010; Parella et al., 2012; Legrand et al., 2016).

https://doi.org/10.5194/egusphere-2022-696
Preprint. Discussion started: 18 October 2022

In this study, we report measurements of ions in surface snow samples collected from several sampling sites (including onshore and offshore sites as well as on the top of a hill) in the high Arctic at Eureka (80°N, 86°W), Nunavut, Canada (Figure 1) during early spring in 2018 and 2019. Surface snow sampling was performed on a daily basis from three layers at depths of 0–0.2 cm, 0.2–0.5 cm, and 0.5–1.5 cm. The low precipitation at Eureka enables us to investigate vertical gradients of salts and ions in the surface layer of snow, and their temporal trend in spring. The data obtained from this study allow us to derive deposition fluxes of bromide and nitrate to surface snow and then investigate the role that snowpack plays as a direct source or sink of reactive bromine and nitrogen. Methods and datasets are described in Section 2. The ionic measurements and snow salinity results are reported in Section 3. Conclusions and atmospheric implications are given in Section 4.

2 Methods and datasets

2.1 Sampling site and local meteorology

Eureka is one of the coldest places in the Canadian Arctic, with average air temperature of -37°C in March. Surface inversions are frequently observed in winter-spring (~84% of the time), and boundary layer height is in the range of 400-800 m (Bradley et al., 1992). Due to the local geography and cold weather, sea ice near the Eureka Weather Station (EWS) is thick (e.g., >1.5 m in March). Satellite-based sea ice data show that there are no clearly identifiable leads or open waters within 600-800 km to the north and west of Eureka in early spring (Bognar et al., 2020). Therefore, the impact of local open leads is negligible. In addition, modelling work shows that this area is only weakly influenced by open ocean sea spray (Rhodes et al., 2017), thus open-ocean sourced bromine influence is secondary (Yang et al., 2020). Under calm weather conditions, the atmospheric boundary layer at Eureka is generally shallow and stratified. Thus the measurements made at the Polar Environment Atmospheric Research Laboratory (PEARL) Ridge Laboratory, located on the top of a hill (610 m asl) (Figure 1) are mainly representative of the free tropospheric influence; however, under unstable condition such as cyclones, PEARL is within the extended boundary layer. In early spring, the UV index changes dramatically from very low levels at the end of February to higher levels at the end of March (Figure S1), mainly due to the rapid increase in daily solar elevation angles after polar sunrise on February 21.

Precipitation in winter-early spring is very low; most snowfall at Eureka happens in the autumn, and snowpack depth does not change much after December. This is consistent with the results of an Arctic snow depth survey by Warren et al. (1999). On sea ice, snowpack depth near shore is 10-30 cm, while snow depth inland varies from only a few cm at convex locations to more than half a meter at concave locations. The type of sea ice in the Slidre Fiord is mainly one-year ice. However, a large iceberg was grounded in the fiord since Summer 2018, which significantly affected 2019 snow salinity and ionic concentrations on sea ice (see below).

https://doi.org/10.5194/egusphere-2022-696
Preprint. Discussion started: 18 October 2022

2.2 Snow sampling

As can be seen from Figure 1, we have several sampling sites between EWS and the PEARL Ridge Lab (hereafter, referred to as PEARL). The two major sampling sites at sea level are ~5 km to the west of EWS: one on sea ice (named "Sea ice," ~100 m offshore) and one onshore (named "Onshore," ~50 m inland). There are two additional inland sites (also close to sea level) just behind EWS: the PEARL "0PAL" (Zero Altitude PEARL Auxiliary Laboratory) site and the "Creek" site which are close together and ~1000 m from the sea ice. PEARL is another major sampling site, which is ~15 km to the west of EWS on top of a hill. In addition, a few snow samples were randomly collected from the Eureka airport (~70 m asl, ~3 km to the east of EWS) and on the sea ice in front of EWS; however, these samples were only analysed for salinity (not ionic concentrations) due to local contamination concerns.

There are two types of surface snow observed at Eureka. One consists of fluffy mobile snow particles, loosely connected and white in colour. They mainly cover the top 0.5 cm of snow, and are a mixture of recent falling snow, drifting snow, and deposited ice crystals. On slightly raised surfaces that face the predominant winds, there is a wind-crust layer that is light brown in colour and hard to break or remove from the surface, representing aged and condensed snow. In 2018, we deliberately collected these two types of surface snow for snow salinity analysis. All samples were collected using their sampling tubes to simply scratch them from the surface, roughly at a depth of 0.3–0.5 cm.

In 2019, we collected the top 1.5 cm snow layer in three sub-layers: 0–0.2 cm, 0.2–0.5 cm, and 0.5–1.5 cm with the aim of investigating the vertical gradient of salts and key ions such as sodium, bromide, and nitrate. A small patch of snowpack at each sampling site was identified where it was covered by soft fluffy snow in the surface layer. We used a small shovel and a funnel for sampling. Daily surface snow samples were collected from Sea ice, Onshore, and PEARL.

In addition to surface snow, airborne snow samples were collected on a daily basis using a mounted tray outside. For example, one tray was mounted outside the 0PAL building, and another one was mounted on the roof of PEARL. The tray is approximately 1 m above the ground at 0PAL, ~1.5 m above the roof, and ~11 m above the ground at PEARL. In windy conditions, most of the samples collected by trays consist of blowing snow particles. In calm conditions, trace samples from deposited ice crystals and growing hoar frost at the edge of the tray can be collected. Falling snow can be clearly sampled in specific conditions.

Column snow samples were collected (at a vertical resolution of 1-3 cm) from a few sampling sites at irregular intervals, but mainly during March 4–12 in both 2018 and 2019. Snow density was measured at a resolution of 3 cm in 2018 using a snow cutter and a hanging scale. The snow density results are shown in Figure S2. Ionic analysis was performed for some column snow samples: three columns from Sea ice and four from Onshore in 2019, and one column from Sea ice and Onshore sites in 2018.

https://doi.org/10.5194/egusphere-2022-696
Preprint. Discussion started: 18 October 2022

2.3 Salinity measurements and ionic analysis

All snow samples collected were transferred to 50 mL polypropylene tubes with screw caps (Corning CentriStar), which prior to field deployment had been rinsed with ultra-high-purity (UHP) water and dried in a class 100 clean laboratory in Cambridge, UK. All tubes with samples were put in a dark bag for temporary storage before moving into ice core boxes for storage and transportation. One set of snow samples were melted in the 0PAL laboratory to measure aqueous conductivity using a conductivity meter (SensIon 5, Hach) with a measurement range of 0–200 $mScm^{-1}$ and a maximum resolution of 0.1 μScm^{-1} at low conductivities (0–199.9 μScm^{-1}). Conductivity values were converted into psu, approximately equivalent to the weight of dissolved inorganic matter in grams per kilogram of seawater. Accuracy as stated by the manufacturer is ±0.001 psu at low salinities (<1 psu). Results are shown in Figure 2.

The 2018 snow samples were shipped frozen back to Cambridge, UK shortly after the campaign, and the 2019 samples were shipped frozen directly to the Canadian Ice Core Lab (CICL) at the University of Alberta. All samples were only melted prior to the ion chromatography (IC) analysis, apart from a small portion of the samples that had been melted for salinity measurements. The 2018 samples were analysed in October 2018 and the 2019 samples were analysed in December 2019. Elevated salinity samples were diluted with UHP water, typically by a factor of 10 or 100 based on the estimated salinity. Due to the presence of fine particulates in the snow samples, all 2019 samples were filtered using Millex-GP Express PES Membrane, Sterile, 33 mm, 0.22 µm filters (Merck Millipore Ltd., Cork, Ireland). The 2018 snow samples were analysed using Thermo Scientific Dionex ICS-4000 ion chromatography systems, with ions of Na^+, Ca^{2+}, Mg^{2+}, K^+, NH_4^+, Cl^-, Br^-, $SO_4^=$, NO_3^-, F^-, acetate, formate, oxalate and MSA measured. The 2019 samples for IC analysis were run on a Dionex ICS-5000+ with ions of Na^+, Ca^{2+}, Mg^{2+}, K^+, Cl^-, Br^-, $SO_4^=$, NO_3^-, and MSA measured. Anion analysis was performed using an ionPac AS18-Fast-4µm column, and cation analysis was performed using an IonPac CS12A column.

Multiple samples (in 2019) were analysed to assess precision. The relative standard deviations of duplicate analyses, limits of detection (LOD, = 3 times standard deviation of filter blank average peak area), and limits of quantification (LOQ, = 10 times standard deviation of filter blank average peak area) for all sequences (~40 samples analysed per sequence) are reported in Table S1. The LOD of Br^- is 16 ppb with a relative standard deviation of 1.8 ppb and the LOD of NO_3^- is 30 ppb with a relative standard of deviation of 2.3 ppb. The mean statistical results for the ionic analysis of the 2018 and 2019 samples are given in Tables S2 and S3, respectively. Mean values excluded outliers, defined as values more than 1.5 interquartile ranges above the upper quartile or below the lower quartile. Column means were calculated using values exclusively within the depth range ≥1.5 and ≤ 20 cm. Interpolation for vertical profile data consisted of 2-cm bin averages from 1.5-cm depth to the bottom of the snowpack.

https://doi.org/10.5194/egusphere-2022-696
Preprint. Discussion started: 18 October 2022

2.4 MAX-DOAS measurements and BrO retrieval

Multi-axis Differential Optical Absorption Spectroscopy (MAX-DOAS) measurements of BrO partial columns were performed at PEARL. Spectra were recorded in the ultra-violet (UV) using a grating spectrometer (spectral resolution 0.45 nm) with a cooled (200 K) charge-coupled device (CCD) detector at 0.4–0.5 nm resolution. Elevation angles of 30°, 15°, 10°, 5°, 2°, 1°, and -1° were used in the elevation scans, and measurements were only taken with solar elevation above 4°. Differential slant column densities (dSCDs) of BrO and the oxygen dimer (O_4) were retrieved using the DOAS technique with the settings described in Zhao et al. (2016) and Bognar et al. (2020). Reference spectra for the DOAS analysis were temporally interpolated from zenith measurements taken before and after each elevation scan. dSCDs were converted to profiles using a two-step optimal estimation method (Frieβ et al, 2011). First, aerosol extinction profiles were retrieved from O_4 dSCDs, and then the extinction profiles were used as a forward model parameter in the BrO vertical profile retrieval. The retrievals were performed for 0–4 km altitude on a grid with 0.2-km resolution. Due to the elevation of the measurement site, the instrument often measures BrO in the free troposphere, except during strong wind episodes and storms that generate a deep boundary layer (Bognar et al., 2020).

2.5 Complementary datasets

There are two sets of local meteorology data used in this work: one from EWS (the archived data are available at Historical Data - Climate - Environment and Climate Change Canada (ECCC) (weather.gc.ca)) and one from PEARL. In addition, ECMWF 6-hourly interim meteorological data (ERA-interim data) were used to explore large-scale weather conditions. Surface ozone measurements were made by a TEI 49i ozone analyzer deployed at 0PAL (Bognar et al., 2020). Hourly mean surface ozone data are available since the instrument was installed in late 2016. The UV index measured during the campaign period in 2018 and 2019 is shown in Figure S1, with data from the ECCC Brewer spectrophotometer (https://doi.org/10.1029/2004JD004820). In addition, NOAA back-trajectory output from the Hybrid Single-Particle Lagrangian Integrated Trajectory (HYSPLIT) model (Stein et al., 2015; Rolph et al. 2017) is used for diagnosing the air-mass history of selected events.

3 Results

3.1 Snow salinities

Figure 2 shows snow salinity distributions over sea ice (purple) and inland (orange) from all measurements, apart from the tray sample results. It can be seen that inland snow has a dual peak distribution with the first and second peaks appearing at 0.001–0.002 psu and 0.01–0.04 psu, respectively. On sea ice, snow has a triple peak distribution, with the first and second peaks overlapping with the inland peaks, indicating similar origins. The third peak at 0.2–0.4 psu clearly reflects sea water contamination.

https://doi.org/10.5194/egusphere-2022-696
Preprint. Discussion started: 18 October 2022

Table 1 shows mean and median snow salinities (psu) in tray samples, at inland and sea ice sites, as well as surface snow (<0.5 cm) salinities at the PEARL, Onshore, and Sea ice sites for two snow types: soft fluffy snow and aged hard snow. Tray samples have the lowest mean value of 0.0070±0.0088 psu (N=14) which is lower than the inland mean (0.0290±0.113 psu, N=211) and the Sea ice mean (0.296±1.640 psu, N=146) by ~4 times and ~40 times, respectively. The lowest daily mean tray sample salinity of 0.00178 psu, obtained on March 6, 2019, corresponded to a falling snow event in calm weather conditions, and is close to the first peak salinity obtained in the surface layer snow, which indicates that the first peak of surface snow salinity (at 0.001-0.002 psu) is likely attributed to the precipitation. The tray samples median of 0.0035 psu is roughly one-third and one-tenth of the inland and sea ice samples median values (0.0115 and 0.0375 psu, respectively, close to their corresponding second salinity peak in Figure 1).

The difference in snow salinity between the two types of surface snow is significant. For example, at PEARL, the mean salinity of the soft fluffy snow is 0.0039±0.0029 psu (N=7), which is ~4 times smaller than that of hard aged snow (0.0175±0.0046 psu (N=2)). At the Onshore site, the difference is ~11-fold (0.00327±0.00273 psu (N=73) vs. 0.0364±0.0112 psu (N=20)). At the Sea ice site, the difference increases to ~23-fold (0.0105±0.0104 psu (N=44) vs. 0.2372±0.3836 psu (N=17)). If we compare these values with the snow salinity distributions in Figure 2, we find that the soft fluffy snow salinity overlaps well with the first peak, and the aged snow salinity overlaps well with the second peak. These results indicate that fresh falling snow and the subsequent condensation effect (via water vapour loss through evaporation/sublimation) may explain the first two salinity peaks in surface snow. The third salinity peak (0.2–0.4 psu) on sea ice is likely due to sea water contamination, which is also observed in the Weddell Sea surface snow (Figure 16 in Frey et al., 2020). In addition, the second snow salinity peak on Eureka sea ice (at 0.02–0.04 psu) is consistent with the Weddell Sea snow salinity on multi-year sea ice, which indicates that the salts on multi-year ice surface layers could be a result of the condensation effect for precipitated salts rather than sea water contamination. However, the Weddell Sea snow salinity does not resolve the first salinity peak (at 0.001–0.002 psu) observed in Eureka, which could be due to the coarse vertical sampling resolution (2-3 cm) applied.

Figure 3 shows surface snow salinity vertical profiles from the first layer (0–0.2 cm) to the third layer (0.5–1.5 cm), and Figure S3 shows column salinity profiles. Note that tray samples salinity is shown in the upper panel of Figure 3. It can be seen that salinity in the third layer (~1 cm) is ~8 and ~15 times that in the first layer at the Onshore site and the Sea ice site, respectively. The larger vertical gradient seen on sea ice is likely due to sea water contamination from below. At PEARL the vertical trend is not clear, perhaps due to the very thin soft fluffy layer (only a few mm) and the thick crust layer observed at the top of the hill where winds are stronger. Generally, tray samples salinity at the 0PAL site is on average larger than that at the PEARL site; we see very similar results in all cations and major anions like [Cl^-] and [NO_3^-] (Figure 4 and S4). The relatively low salinity at the PEARL site is likely attributed to two factors: the higher geographic altitude (~600 m) and the higher height of the mounted tray above the ground (e.g., ~11 m at PEARL versus ~1 m at 0PAL). Therefore, there are less impacts from the sea-ice sourced salts as well as from blowing/drifting snow.

The column salinity profiles in Figure S3 are predominantly 2018 data. Snow salinities at all inland sites do not vary much with distance from the surface. PEARL has the lowest column mean salinity (0.0023±0.0019 psu). Onshore has >10 times the

https://doi.org/10.5194/egusphere-2022-696
Preprint. Discussion started: 18 October 2022

salinity (0.036±0.034 psu). The highest column mean snow salinity was observed on sea ice in 2018, with a mean value (top 20 cm) of 1.673±2.09 psu and a maximum salinity of 18.73 psu at the bottom of the snowpack. It is interesting to note that the 2019 column mean salinity on sea ice (top 20 cm) is very low (0.085±0.026 psu), about 20 times lower than the 2018 value, which is clearly attributed to the dilution effect from the large iceberg grounded near Eureka.

3.2 Ion concentrations and vertical profiles

Figure 4 shows vertical profiles of 2019 ions [Na^+], [Cl^-], [NO_3^-], [Br^-], non-sea-salt bromide (noted as nss[Br^-] =[Br^-]$_{obs}$-0.00625×[Na^+]$_{obs}$), non-sea-salt [SO_4^{2-}] (nss[SO_4^{2-}]=[SO_4^{2-}]$_{obs}$-0.251×[Na^+]$_{obs}$) and enrichment factors of Br^-, Cl^- and SO_4^{2-}. Non-sea-salt values are calculated with the aim of removing salt effects on the concentration of bromine and sulphate, which assists data interpretation particularly in comparisons between offshore and onshore sites as well as from different snow depths. The enrichment factor is calculated following the equation of $EF_X=([X]/[Na]_{obs})/([X]/[Na]_{seawater})$, where $[X]/[Na]_{obs}$ represents the mass ratio of ion X to sodium in a sample, and $[X]/[Na]_{seawater}$ is the ratio in standard sea water. If EF_Y >1.0, ion X is enriched and if <1.0 it is depleted. To highlight the surface snow results, a lognormal Y-axis is applied. Tray sample results are plotted in the top panel of each plot. Figure S4 shows the remaining profiles, including [Ca^{2+}], [Mg^{2+}], [K^+], [SO_4^{2-}] and enrichment of [Ca^{2+}], [Mg^+] and [K^+].

As can be seen from Figure 4(a) and data in Table S3, the tray sample mean [Na^+] is on average 1.7 and 1.2 times of that of the first layer result at PEARL and 0PAL, respectively. For [Cl^-] (Figure 4(b)), this factor is 1.5 and 1.3 times at PEARL and 0PAL, respectively. The enhancement of tray sample salts is likely due to the water loss via sublimation processes. However, this condensation effect cannot explain the even larger enhancement in [NO_3^-] and nss[Br^-] seen in Figure 4(c) and (e), respectively. For instance, the tray sample mean [NO_3^-] at 0PAL is 3.6 times the first layer mean, and 2.1 times at PEARL. Tray sample nss[Br^-] at 0PAL is 2.6 times the first layer mean. This indicates that airborne snow particles may uptake more gaseous nitric acid and soluble bromine species from the air than snow on the ground.

Similar to snow salinity profiles (in Figure 3), 2019 surface snow [Na^+] (and [Cl^-]) increases significantly from the first layer to the third layer, e.g., by about 20-fold at Onshore, 30-fold at Sea ice, and 8-fold at PEARL (in Figure 4(a) and (b)). The lowest sodium concentrations in the first layer are likely due to the precipitation dilution effect. [Br^-] and [$SO_4^=$] in Figure4(e) and (i) both show a similar large vertical gradient, however nss[Br^-] and nss[$SO_4^=$] do not show such a trend (Figure 4(d) and (f)) indicating the ions' enhancement is associated with the water condensation effect. A similar level of nss[Br^-] (of 20–30 ppb) is found at Sea ice and Onshore, strongly indicating they are similarly affected by atmospheric bromine species. The positive nss[Br^-] values also indicate that surface snow is a net sink of atmospheric bromine prior to the measurements. At PEARL, positive nss[Br^-] is only observed in tray and top 0.5 cm snow (with values of 22.7, 21.5 and 0.3 ppb in the tray samples, first and second layers, respectively). Negative nss[Br^-] is obtained in a deep layer, e.g., with a column mean of -3.5 ppb (Table S3), indicating snowpack at the top of the hill is bromide depleted. However, due to the lack of temporal variation information, we cannot determine when this bromine depletion occurs (e.g., before or after the precipitation) or more precisely whether the depletion occurred recently after sunrise. However, 2018 snow at PEARL does not show such bromine depletion;

https://doi.org/10.5194/egusphere-2022-696
Preprint. Discussion started: 18 October 2022

instead it shows a small positive column mean nss[Br^-] of 0.9 ppb (Table S2), which is consistent with the 2018 nss[Br^-] profile shown in Figure S5(d).

Figure 4(g-i) shows the enrichment factor for Br^-, Cl^- and SO_4^{2-} in 2019 snow samples. It can be seen that they are significantly enriched in the surface layer and in tray samples. In particular, we find EF_{Br^-} >10 in tray samples and the first and second layer at the Onshore and Sea ice sites. Similar results were reported at an inland Arctic site (Simpson et al., 2005) and on first-year sea ice (Peterson et al., 2019). Since we do not have simultaneous measurements of soluble inorganic bromine or filter aerosols, we cannot derive robust conclusions regarding their form of deposition to the surface.

2018 vertical profiles (e.g., [Na^+], [NO_3^-], [Br^-] and nss[Br^-]) are shown in Figure S5. Comparing to 2019 snow profiles, 2018 column sodium and bromide are much higher. For instance, column mean (1.5–20 cm) bromide concentration on sea ice is 858.4 ppb in 2018 (Table S2) and 576.7 ppb in 2019 (Table S3). The lower 2019 bromide in snowpack on sea ice is due to the fresh water dilution effect by the grounded iceberg. However, surface snow bromide does not follow this pattern; instead, the 2018 surface bromide is even lower than that of the 2019 values. For example, bromide mean in the top 0.5 cm snow layer in 2018 is only 18.2 ppb (Table S2), which is significantly lower than the 2019 surface bromide with mean values of 32.0 and 242.3 ppb in the 0–0.2 cm and 0.2–0.5 cm layers, respectively (Table S3). The lower 2018 surface bromide loading is likely related to the extremely low BrO partial columns measured in March 2018 at Eureka by MAX-DOAS (Bognar et al., 2020), during which unusually calm weather, low aerosol optical depth (AOD) and coarse-mode aerosol (likely SSA) concentrations were observed (see Section 3.3 and Figure 5 below for more details). These results indicate that top layer snow bromide is largely controlled by atmospheric processes rather than by underlying snowpack. This conclusion is also consistent with previous finding that bromide concentrations at low salinities are dominated by atmospheric exchange (Krnavek et al., 2012). Interestingly, surface layer nitrate concentrations between 2018 and 2019 are not significantly different.

3.3 Time series of surface snow [NO_3^-] and [Br^-]

Figure 5 shows the 2018 time series of local meteorology (temperature and daily precipitation in (a), air pressure and wind speeds in (b)), 1-hourly surface ozone at 0PAL and 0-4 km BrO partial column (c), and top 0.5 cm snow [Na^+] (d), [NO_3^-] (e), [Br^-] (f), and nss[Br^-] (g) at the Sea ice, Onshore, and PEARL sites. Figure 6 shows the 2019 time series of meteorology at the EWS (a-b), surface ozone at 0PAL and 0-4 km BrO partial column (c), and tray samples [Na^+] (d), [NO_3^-] (e), [Br^-] (f), and nss[Br^-] (g) at the 0PAL and PEARL sites. Figure 7 shows the 2019 time series of surface snow nitrate (a-c) and bromide (d-f) in three sub-layers: 0–0.2 cm, 0.2–0.5 cm, and 0.5–1.5 cm.

We observe extremely calm conditions with wind speeds <5 m s^{-1} most days in March 2018, with strong inversions between EWS and PEARL (e.g., the temperature difference between these two heights can be >10°C, Figure 5(a)). Blowing snow events were only recorded on March 3 and 5, 2018 which is unusually infrequent. On the contrary, March 2019 was very windy, with blowing snow events recorded on March 1, 2, 4, 12–14, 18, 19, 23–25, and 28, 2019, approximately 40% of the days.

https://doi.org/10.5194/egusphere-2022-696
Preprint. Discussion started: 18 October 2022

March 2018 has very low background BrO partial columns of ~1×10^{13} molecules cm^{-2} or less (Figure 5(c)), while March 2019 has a background BrO partial column almost two times the 2018 level (Figure 6(c)). Accordingly, surface ozone concentrations in March 2018 are generally higher than in March 2019. Apart from the ODE occurrence, surface ozone in March 2018 is mainly around 30 ppbv, while in March 2019 surface ozone is mainly below 20 ppbv indicating accelerated ozone losses due to enhanced BrO loading in the air.

Here we focus on the 2019 datasets (Figures 6 and 7) for further discussion. By examining the meteorology record we find that fog events are recorded on March 7, 15, 17-20, 22, and 28, 2019. Some of these events are accompanied by precipitation (daily amount ≥0.2 mm, as shown in Figure 6(b), on March 5, 6, 7, 10, 15, 19, 27, 28, 30, and 31, with total monthly precipitation of 2 mm). In addition, trace precipitation days (daily amount of zero) were recorded on March 1, 2, 4, 11, 12, 18, 20, and 21. If all precipitation days are taken into account, a mean snowfall frequency of 1.7 days is obtained. Ice crystals are another very common phenomenon in Eureka during calm weather.

Tray sample sodium has a large day-to-day variability (Figure 6(d)). The low sodium concentrations observed on March 6 and 11, 2019 are likely attributed to precipitation dilution effects, with the high sodium concentrations measured on March 4–5, 13–14, and 24 related to very windy conditions. In general, tray sample sodium does not show a clear increase at 0PAL, though this is evident at PEARL.

Tray sample nitrate at 0PAL shows a clear increasing trend with a mean slope of 10.95 ppb d^{-1} (correlation coefficient R=0.46) (Figure 6(e)). A similar increasing trend in nitrate can be seen in all three sub-layers except at PEARL (Figure 7). For instance, nitrate in the first layer (0–0.2 cm) snow has a slope of 15.7 ppb d^{-1} (R=0.50) at the Sea ice site and 16.7 ppb d^{-1} (R=0.48) at the Onshore site. In the second layer (0.2–0.5 cm), the nitrate slope is 14.6 ppb d^{-1} (R=0.70) at the Sea ice site and 10.2 ppb d^{-1} (R=0.52) at the Onshore site. In the third layer (0.5–1.5 cm), the slope is smaller: 3.6 ppb d^{-1} (R=0.41) at the Sea ice site and 5.0 ppb d^{-1} (R=0.51) at the Onshore site. These values are only 1/5 to 1/3 of the top two-layer values, indicating a reduced nitrate deposition flux to deeper snow.

Nitrate at PEARL behaves differently. For instance, a near zero increasing trend is observed in tray samples and in the first layer (Figure 6(e) and 7(a)). Moreover, a negative slope can be seen in the second and third layers, with values of -1.0 ppb d^{-1} (R=0.29) and -3.33 ppb d^{-1} (R=0.80), respectively. These results indicate that deposition flux at the top of the hill is reduced and cannot compensate for nitrate loss via photolysis. It is reasonable to assume snow at sea level has a similar nitrate loss via photolysis, however the positive trends indicate that local snow in the fiord has a net effect of absorbing reactive nitrogen from the air.

Due to the large enrichment factor of bromide in surface snow samples, surface sample [Br^-] and nss[Br^-] both show a very similar increasing trend (Figure 6(f) verse 6(g)). The 2019 slope of nss[Br^-] in tray samples is 1.83 ppb d^{-1} (R=0.64) at 0PAL and 1.03 ppb d^{-1} (R=0.56) at the PEARL site. Figure 7(d) shows the first layer nss[Br^-] slope is 1.96 ppb d^{-1} (R=0.50) at Sea ice, 1.84 ppb d^{-1} (R=0.56) at the Onshore site, and 0.94 ppb d^{-1} (R=0.65) at the PEARL site. The second layer nss[Br^-] slope (Figure 7(e)) is slightly smaller: 1.46 ppb d^{-1} (R=0.42) at Sea ice, 1.12 ppb d^{-1} (R=0.39) at the Onshore site, and 1.39 ppb d^{-1}

https://doi.org/10.5194/egusphere-2022-696
Preprint. Discussion started: 18 October 2022

(R=0.67) at the PEARL site. However, due to the limited available data in the third layer we could not derive a robust trend, but the Onshore dataset indicates a near zero slope (Figure 7(f)).

Both nitrate and bromide show a large day-to-day perturbation. For instance, the maximum nitrate concentration of ~1000 ppb observed on March 18, 2019 (in tray samples and the first layer) is clearly associated with a heavy fog event. Meanwhile, that day is also coincident with an enhanced bromide concentration (~100 ppb). Another enhancement of bromide on March 22, 2019 (in tray samples) also corresponds to a fog event. We do not detect clear precipitation effects on nitrate, and this could be due to the fact that nitrate in precipitation is very similar to that in the surface layer snow. However, we do see large precipitation dilution effects on surface bromide as observed on March 5, 6, 10, 11, 20, and 21, 2019.

We do not see a clear correlation between surface snow sodium and bromide at Eureka, indicating that enhanced sodium does not necessarily accompany enhanced bromide. However, on a very windy day or shortly after a storm, such as on March 4, 14 and 24, 2019, both high bromide and sodium were observed, indicating locally sourced contribution.

As noted above, March 18, 2019 was a heavy fog day. The signals of extremely high nitrate on that day can be clearly seen in tray samples and the first layer, but still slightly detected in the second layer at the Onshore site (Figure 7(a-b)). However, the signal disappears in the third layer, indicating the fog-related nitrate deposition is confined to the skin layer and limited to the mobile fluffy snow layer. Snowpack is a highly permeable material, and the exchange of air with the atmosphere (Sturm and Johnson, 1991; Albert and Hardy, 1995; Colbeck, 1997; Albert et al., 2002) means gasses and fine aerosols could penetrate into deep layers (Harder et al., 1996; Björkman, et al., 2013). However, our data indicate that fog particles may not penetrate efficiently into a deep layer and most deposited nitrate is limited to a depth of 0.5 cm.

The 2018 time series dataset shows a similar story to the 2019 dataset. For example, top 0.5 cm snow nitrate shows a similar slope of 14.88 ppb d^{-1} (R=0.93) at the Sea ice site and 10.31 ppb d^{-1} (R=0.61) at the Onshore site. However, 2018 nss[Br^-] does not show a clear increasing trend, with a slope of 0.37 ppb d^{-1} (R=0.27) at Sea ice (and 0.09 ppb d^{-1} (R=0.07) at Onshore) (Figure 5(g)). This small slope is only 1/4 to 1/3 of the 2019 slope, indicating a reduced bromide deposition flux. Although 2018 snowpack column mean bromide on sea ice is several times the 2019 column mean, the low bromide deposition flux to surface snow in 2018 is attributed to the calm weather and the extremely low BrO loading as measured by MAX-DOAS (Bognar et al., 2020).

3.4 Deposition flux of bromide and nitrate

The daily slopes of nitrate and bromide derived above can be used to calculate their deposition flux to snowpack following this new equation:

$$Flux = \frac{A}{MT}\sum_{k=1}^{n} S_k H_k D_k \quad \text{(R3)}$$

where *Flux* is integrated deposition flux (in units of molecules cm^{-2}) from snow layer 1 to n, A is Avogadro's number of gas (6.02×10^{23} molecules $mole^{-1}$), M is mole weight of species (nitrate or bromide) in grams, T is seconds in 1 day (86400 s d^{-1}),

https://doi.org/10.5194/egusphere-2022-696
Preprint. Discussion started: 18 October 2022

S_k is the derived daily slope in snow layer k (in ppb d^{-1}), H_k is the corresponding snow layer depth (in cm), and D_k is snow density of the layer (in g cm^{-3}).

In this study, n=3. A low snow density of 0.15 g cm^{-3} is used for the top two layers, and 0.3 g cm^{-3} is used for the third layer. For nitrate, we use a mean slope value (from the Sea ice and Onshore sites) of 12.1, 12.4, and 4.3 ppb d^{-1} in the first, second, and third layers, respectively. Therefore, we calculate an integrated nitrate deposition flux of 2.4×10^8 molecules cm^{-2} s^{-1} from the top 1.5 cm snow. At PEARL, the integrated deposition flux is -1.0×10^8 molecules cm^{-2} s^{-1} (according to a mean slope of 0.0, -1.0, and -3.3 ppb d^{-1} in the three sub-layers). These results indicate that surface snow at sea level is a net sink of atmospheric nitrate, and at the top of the hill is a source of reactive nitrate.

For bromide, the integrated deposition flux to the top 1.5 cm layer snow is 1.29×10^7 molecule cm^{-2} s^{-1} at sea level (using a mean slope of 1.9, 1.3, and 0.0 ppb d^{-1} in the three sub-layers, respectively). At PEARL, the integrated flux is 1.01×10^7 molecules cm^{-2} s^{-1} which is ~20% lower than at sea level. This small vertical gradient strongly indicates that BrO concentrations (and total inorganic bromine species) within the boundary layer and in the free troposphere are not significantly different at Eureka, which is in agreement with the conclusion in Bognar et al. (2020). This implies either that bromine species at Eureka are well mixed in the lower troposphere or local snowpack at sea level is not a large source of reactive bromine. As mentioned previously, from winter to early spring the boundary layer in Eureka is very shallow and stratified in calm conditions, thus most of the time PEARL is located in the free troposphere. Therefore, if local snowpack on sea ice in the fiord is a large source of reactive bromine, an enhanced deposition flux at sea level will be detected. In addition, previous work focusing on atmospheric chemistry has demonstrated that large BrO enhancement events observed at Eureka in early spring are mostly transported via cyclones (Zhao et al., 2016; 2017; Yang et al., 2020). The transported bromine in association with storms means well-mixed bromine species from the surface up to high altitudes (> 1 km), which explains the small vertical gradient of deposited bromine flux measured in this current work. The observed ODE and BEE measured during March 6–10, 2018, for example, is associated with a transported cyclone event (to be addressed in a separate study).

3.5 Relationship between surface snow [NO_3^-] and [Br^-]

No significant relationship is found between sodium and bromide or between sodium and nitrate in surface snow. However, we do find a significant relationship between surface snow [NO_3^-] and [Br^-] (Figure 8) in tray samples at 0PAL, 0–0.2 cm, and 0.2–0.5 cm layer snow at the Onshore site (2019), and the top 0.5 cm snow at the Onshore site (2018), with coefficient R in the range of 0.4-0.7. This relationship remains when nss[Br^-] is used in the analysis with a similar R of 0.23–0.66 (Figure S6). Moreover, the ratio of [NO_3^-]/[Br^-] ranges from 3.5–6.8, indicating that one molecule bromide deposited to surface snow is likely accompanied by 4–7 nitrate molecules. For the first time we see field evidence on a time scale of one day showing this effect. This finding further confirms previous conclusions regarding the role that reactive bromine plays in determining high latitude atmospheric reactive nitrogen (e.g., Yang et al., 2005; Morin et al., 2008). We do not see such a relationship in snow on sea ice, likely due to sea water contamination of bromide. However, we do see a weak correlation at PEARL (not shown).

https://doi.org/10.5194/egusphere-2022-696
Preprint. Discussion started: 18 October 2022

4 Conclusions

Based on two years of daily surface snow sampling in the Canadian high Arctic, we derive an integrated spring nitrate deposition flux of 2.4×10^8 molecules cm^{-2} s^{-1} from the top 1.5 cm of the snowpack at sea level. At the top of the hill (PEARL, ~600 m), surface snow has a negative deposition flux of -1.0×10^8 molecules cm^{-2} s^{-1}, indicating surface snow is losing nitrate in early spring. The integrated bromide deposition flux at sea level is 1.29×10^7 molecules cm^{-2} s^{-1}, which is ~10 times smaller than that of the nitrate flux. At PEARL, the integrated deposition flux is very similar to the flux at sea level (only 22% smaller). This small vertical gradient between the boundary layer and the free troposphere implies that snowpack at Eureka is not a large source of reactive bromine, although the nitrate flux gradient data strongly indicate that local snowpack could serve as a source of reactive nitrogen.

If we assume that nitrate and bromide deposited to the snow surface are roughly balanced by the emission flux of reactive nitrogen and bromine from the local snowpack, we can then derive a local snowpack emission flux of $\sim1\times10^7$ molecules cm^{-2} s^{-1} for reactive bromine and 2.4×10^8 molecules cm^{-2} s^{-1} for reactive nitrogen. Compared to previous snowpack emission fluxes of reactive bromine, we find that our derived flux is smaller by more than an order of magnitude. This means that local snowpack is only a weak source of reactive bromine and should not be able to cause BEEs or ODEs in polar spring, but rather influence background BrO. On the contrary, our derived reactive nitrate flux is well within the range of previously estimated fluxes, which suggests that the approach applied in this study is effective.

It has been previously shown that the typical time needed for a surface signal to reach the upper area in a stable boundary layer is 7–30 hrs (Stull, 1988). Therefore, the one-day timescale selected for sampling may allow sufficient time for emitted chemical species to mix well in the boundary layer and reach a rough equilibrium state with other processes, including depositions and photochemistry. The derived deposition flux only represents a lower end of possible fluxes. This is because when samples are collected at a one-day interval, some chemically active species may reach a photochemical state after deposition and re-emission. In addition, samples were only collected from the top 1.5 cm snow layer, so the deposition flux may be underestimated. For example, if the nitrate slope obtained in the 0.5-1.5 cm is applied to the 1.5-5 cm snow layer, then the total nitrate deposition flux derived will be roughly tripled.

Another finding of this study is that surface snow (<0.5 cm) nitrate and bromide are significantly correlated with a $[NO_3^-]/[Br^-]$ ratio of 4–7. This means reactive bromine could effectively accelerate NO_X-to-nitrate conversion. This is the first time such an effect has been seen on a timescale of one day. This also reinforces the importance of reactive bromine in polar and high latitude reactive nitrogen budgets, and its atmospheric oxidising capacity.

Author Contributions

XY designed the field experiment and performed snow sampling, salinity measurements, and data interpretation. KS and KAW co-organised the campaign. PF and the Canadian Network for the Detection of Atmospheric Change (CANDAC) team provided logistics support and performed snow sampling. AC led ion chromatography analysis for the 2019 samples. KB

https://doi.org/10.5194/egusphere-2022-696
Preprint. Discussion started: 18 October 2022

provided MAX-DOAS BrO data, SMM and PE provided surface ozone data, and XZ supplied local meteorology and radiation data. MGS performed major ionic analysis and plotting. XY led the writing with contributions from all co-authors.

Competing Interest

The authors declare that they have no conflict of interest.

Data Availability

All the data will be archived in BAS Polar Data Centre.

Acknowledgements

We thank the UK NERC Arctic office for their support to this study via two UK-Canada bursary programs: "The role of tundra snowpack chemistry in the boundary layer bromine budget at Eureka, Canada" (2018), and "A second investigation of the role of tundra snowpack chemistry in the boundary layer 'bromine explosion'" (2019). The Eureka MAX-DOAS BrO measurements were made at the PEARL Ridge Laboratory by CANDAC, primarily supported by NSERC, CSA, and ECCC. The UV index data are from Brewer spectrophotometer by Environment and Climate Change Canada (ECCC). We thank CANDAC and ECCC for enabling and supporting the snow sampling campaigns and BAS Ice Core Laboratory for analysing the 2018 samples (by Sara L. Jackson). The NOAA Arctic Research Program, Physical Sciences Laboratory, and Global Monitoring Laboratory have contributed to establishing surface ozone measurement programs in Eureka.

References

Abbatt, J. P. D.: Interaction of HNO_3 with water-ice surfaces at temperatures of the free troposphere, *Geophys. Res. Lett.* 24, 1479-1482, 1997.

Abbatt, J. P. D., Thomas, J. L., Abrahamsson, K., Boxe, C., Granfors, A., Jones, A. E., King, M. D., Saiz-Lopez, A., Shepson, P. B., Sodeau, J., Toohey, D. W., Toubin, C., von Glasow, R., Wren, S. N., and Yang, X.: Halogen activation via interactions with environmental ice and snow in the polar lower troposphere and other regions, *Atmos. Chem. Phys*., 12, 6237-6271, https://doi.org/10.5194/acp-12-6237-2012, 2012.

Albert, M. R. and Hardy, J. P.: Ventilation experiments in a seasonal snow cover. Biogeochemistry of Seasonally Snow Covered Catchments, IAHS pub. No. 228, 44-49, 1995.

Albert, M. R., Grannas, A. M., Bottenheim, J., Shepson, P. B. and Perron, F. E.: Processes and properties of snow-air transfer in the high Arctic with application to interstitial ozone at Alert, Canada, *Atmos. Environ*., 36, 2779-2787, 2002.

https://doi.org/10.5194/egusphere-2022-696
Preprint. Discussion started: 18 October 2022

Angot, Helene, Dastoor, Ashu, De Simone, Francesco, Gardfeldt, Katarina, Gencarelli, Christian N., Hedgecock, Ian M., Langer, Sarka, Magand, Olivier, Mastromonaco, Michelle N., Nordstrom, Claus, Pfaffhuber, Katrine A., Pirrone, Nicola, Ryjkov, Andrei, Selin, Noelle E., Skov, Henrik, Song, Shaojie, Sprovieri, Francesca, Steffen, Alexandra, Toyota, Kenjiro, Travnikov, Oleg, Yang, Xin, Dommergue, Aurelien.: Chemical cycling and deposition of atmospheric mercury in Polar Regions: review of recent measurements and comparison with models, *Atmospheric Chemistry and Physics*, 16. 10735-10763. 10.5194/acp-16-10735-2016, 2016.

Barrie, L. A., Bottenheim, J. W., Schnell, R. C., Crutzen, P. J., and Rasmussen, R. A.: Ozone destruction and photochemical reactions at polar sunrise in the lower Arctic atmosphere, *Nature*, 334, 138–141, https://doi.org/10.1038/334138a0, 1988.

Beine, H. J., Honrath, R. E., Dominé, F., Simpson, W. R., & Fuentes, J. D.: NO_x during background and ozone depletion periods at Alert: Fluxes above the snow surface, *Journal of Geophysical Research*, 107(D21), 12. https://doi.org/10.1029/2002JD002082, 2002.

Beine, H. J., Dominè, F., Ianniello, A., Nardino, M., Allegrini, I., Teinilä, K., and Hillamo, R.: Fluxes of nitrates between snow surfaces and the atmosphere in the European high Arctic, *Atmos. Chem. Phys*., 3, 335–346, https://doi.org/10.5194/acp-3-335-2003, 2003.

Björkman, RAFAEL Kühnel, DANIELG. Partridge, TJARDAJ. Roberts, WENCHE Aas, MAURO Mazzola, ANGELO Viola, ANDY Hodson, JOHAN Ström & ELISABETH Isaksson: Nitrate dry deposition in Svalbard, *Tellus B: Chemical and Physical Meteorology*, 65:1, 19071, DOI: 10.3402/tellusb.v65i0.19071, 2013.

Bloss, W.J., Lee, J.D., Heard, D.E., Salmon, Bauguitte, S.J.-B., Roscoe, H.K., Jones, A.E.: Observations of OH and HO_2 radicals in coastal Antarctica, *Atmos. Chem. Phys*., 7, 4171-4185, 2007.

Bloss, W., Camredon, M., Lee, J.D., Heard, D.E., Plane, J.M.C., Saiz-Lopez, A., Bauguitte, S.J.B., Salmon, R.A., & Jones, A.E.: Coupling of Hox, NOx and halogen chemistry in the 16 odelling boundary layer, *Atmospheric Chemistry and Physics*, *10*(21), 10187-10209. https://doi.org/10.5194/acp-10-10187-2010, 2010.

Bognar, K., Zhao, X., Strong, K., et al.: Measurements of tropospheric bromine monoxide over four halogen activation seasons in the Canadian high Arctic, *J. Geophys. Res. Atmos*. 125, doi:10.1029/ 2020JD033015, 2020.

Bottenheim, J. W., Gallant, A. G. & Brice, K. A.: Measurements of NO_y species and O_3 at 82°N latitude, *Geophys. Res. Lett.* 13, 113–116, 1986.

Bradley, Raymond S.; Keimig, Frank T.; Diaz, Henry F.: Climatology of Surface-Based Inversions in the North American Arctic, *Journal of Geophysical Research*, 97, D14, 15,699-15,712, DOI: 10.1029/92JD01451, 1992.

Brough, Neil; Jones, Anna E.; Griffiths, Paul T.: Influence of sea-ice-derived halogens on atmospheric Hox as observed in springtime coastal Antarctica, *Geophysical Research Letters*, 46 (16). 10168-10176. https://doi.org/10.1029/2019GL083825, 2019.

Chan, H. G., King, M. D., & Frey, M. M.: The impact of parameterising light penetration into snow on the photochemical production of NO_x and OH radicals in snow, *Atmospheric Chemistry and Physics*, 15(14), 7913– 7927. https://doi.org/10.5194/acp-15-7913-2015, 2015.

https://doi.org/10.5194/egusphere-2022-696
Preprint. Discussion started: 18 October 2022

Chan, H. G., Frey, M. M., and King, M. D.: Modelling the physical multiphase interactions of HNO_3 between snow and air on the Antarctic Plateau (Dome C) and coast (Halley), *Atmos. Chem. Phys*., 18, doi:10.5194/acp-18-1507-2018, 2018.

Colbeck, S. C.: Model of wind pumping for layered snow, *J. Glaciol*., 43, 60-65, 1997.

Custard K. D., A. R. W. Raso, P. B. Shepson, R. M., Staebler, and K. A. Pratt, Production and release of molecular bromine and chlorine from the Arctic coastal snowpack, *ACS Earth and Space Chemistry*, 1(3), 142-152, https://doi.org/10.1021/acsearthspacechem.7b00014, 2017.

Criscitiello, A. S., Geldsetzer, T., Rhodes, R. H., Arienzo, M., McConnell, J., Chellman, N., et al. (2021). Marine aerosol records of Arctic sea-ice and polynya variability from new Ellesmere and Devon Island firn cores, Nunavut, Canada. Journal of Geophysical Research: Oceans, 126, e2021JC017205.https://doi.org/10.1029/2021JC017205.

Dickerson, R. R. 1985. Reactive nitrogen-compounds in the Arctic. *J. Geophys. Res.-Atmos*. 90, 1073910743.

Diehl, K., Mitra, S. K. and Pruppacher, H. R.: A laboratory study of the uptake of HNO3 and HCL vapor by snow crystals and ice spheres at temperatures between 0 and -40°C, *Atmos. Environ*. 9, 975-981. DOI: 10.1016/1352-2310(95)00022-q, 1995.

Dubowski, Y., Colussi, A. J., and Hoffmann, M. R.: Nitrogen dioxide release in the 302 nm band photolysis of spray-frozen aqueous nitrate solutions: Atmospheric Implications, *J. Phys. Chem*., A, 105, 4928–4932, 2001.

Domine, F., A. S. Taillandier, W. R. Simpson, and K. Severin: Specific surface area, density and microstructure of frost flowers, *Geophys.Res. Lett*., 32, L13502, doi:10.1029/2005GL023245, 2005.

Falk, S. and Sinnhuber, B.-M.: Polar boundary layer bromine explosion and ozone depletion events in the chemistry–climate model EMAC v2.52: implementation and evaluation of AirSnow algorithm, *Geosci. Model Dev*., 11, 1115–1131, https://doi.org/10.5194/gmd-11-1115-2018, 2018.

Frieß, U., Sihler, H., Sander, R., Pöhler, D., Yilmaz, S., and Platt, U.: The vertical distribution of BrO and aerosols in the Arctic: Measurements by active and passive differential optical absorption spectroscopy, J. Geophys. Res.-Atmos., 116, D00R04, https://doi.org/10.1029/2011JD015938, 2011.

Frey, M. M., et al.: The diurnal variability of atmospheric nitrogen oxides (NO and NO_2) above the Antarctic Plateau driven by atmospheric stability and snow emissions, *Atmos. Chem. Phys.* 13, doi:10.5194/acp-13-3045-2013, 2013.

Frey, Markus M. , Norris, Sarah J., Brooks, Ian M., Anderson, Philip S., Nishimura, Kouichi, Yang, Xin , Jones, Anna E. , Nerentorp Mastromonaco, Michelle G., Jones, David H., Wolff, Eric W.: First direct observation of sea salt aerosol production from blowing snow above sea ice. *Atmospheric Chemistry and Physics*, 20. 2549-2578. 10.5194/acp-20-2549-2020, 2020.

Harder, S. L., Warren, S. G., Charlson, R. J. and Covert, D. S.: Filtering of air through snow as a mechanism for aerosol deposition to the Antarctic ice sheet, *J. Geophys. Res.-Atmos*., 101, 18729-18743, 1996.

Hoffmann, E. H., Tilgner, A., Schrödner, R., Bräuer, P., Wolke, R., and Herrmann, H.: An advanced 17odelling study on the impacts and atmospheric implications of multiphase dimethyl sulfide chemistry, *P. Natl. Acad. Sci*., USA, 113, 11776–11781, https://doi.org/10.1073/pnas.1606320113, 2016.

Holmes, C. D., Jacob, D. J., and Yang, X.: Global lifetime of elemental mercury against oxidation by atomic bromine in the free troposphere, *Geophys. Res. Lett*., 33, L20808, doi:10.1029/2006GL027176, 2006.

https://doi.org/10.5194/egusphere-2022-696
Preprint. Discussion started: 18 October 2022

Honrath, R. E., Lu, Y., Peterson, M. C., Dibb, J. E., Arsenault, M. A. and co-authors: Vertical fluxes of NOx, HONO, and HNO_3 above the snowpack at Summit, Greenland, *Atmos. Environ*. 36, 2629-2640, 2002.

Huang, J., Jaeglé, L., Chen, Q., Alexander, B., Sherwen, T., Evans, M. J., et al.: Evaluating the impact of blowing-snow sea salt aerosol on springtime BrO and O3 in the Arctic, *Atmospheric Chemistry and Physics*, 20(12), 7335–7358. https://doi.org/10.5194/acp-20-7335-2020, 2020.

Jones, A. E., Weller, R., Anderson, P. S., Jacobi, H.-W., Wolff, E. W., Schrems, O., & Miller, H.: Measurements of NO_x emissions from the Antarctic snowpack. *Geophysical Research Letters*, 28(8), 1499– 1502. https://doi.org/10.1029/2000GL011956, 2001.

Kaleschke, L., et al.: Frost flowers on sea ice as a source of sea salt and their influence on tropospheric halogen chemistry, *Geophys. Res. Lett.*, 31, L16114, doi:10.1029/2004GL020655, 2004.

Kirpes, R. M., Bonanno, D., May, N. W., Fraund, M., Barget, A. J., Moffet, R. C., & Pratt, K. A.: Wintertime Arctic sea spray aerosol composition controlled by sea ice lead microbiology, *ACS Central Science*, 5(11), 1760– 1767. https://doi.org/10.1021/acscentsci.9b00541, 2019.

Krnavek, L., Simpson, W. R., Carlson, D., Domine, F., Douglas, T. A., and Sturm, M.: The chemical composition of surface snow in the Arctic: Examining marine, terrestrial, and atmospheric influences. *Atmospheric Environment*, 50(0):349–359. ISSN 13522310. http://www.sciencedirect.com/science/article/pii/S1352231011012192. DOI: https://doi.org/10.1016/j.atmosenv.2011.11.033, 2012.

Lehrer, E.; Hönninger, G.; Platt, U.: A One Dimensional Model Study of the Mechanism of Halogen Liberation and Vertical Transport in the Polar Troposphere, *Atmos. Chem. Phys*., 4, 2427−2440, 2004.

Legrand, M., Yang, X., Preunkert, S., and Theys, N.: Year-round records of sea salt, gaseous, and particulate inorganic brominein the atmospheric boundary layer at coastal (Dumont d'Urville) and central (Concordia) East Antarctic sites, *J. Geophys. Res.-Atmos*., 121,997–1023, doi:10.1002/2015JD024066, 2016.

Marelle, L., Thomas, J. L., Ahmed, S., Tuite, K., Stutz, J., Dommergue, A., Simpson, W. R., Frey, M. M. and Baladima, F.: Implementation and Impacts of Surface and Blowing Snow Sources of Arctic Bromine Activation Within WRF-Chem 4.1.1, *J. Adv. Model. Earth Syst*., 13, 8, e2020MS002391, doi:10.1029/2020ms002391, 2021.

Morin, S., Savarino, J., Frey, M. M., Yan, N., Bekki, S., Bottenheim, J. W., and Martins, J. M. F.: Tracing the origin and fate of NO_x in the Arctic atmosphere using stable isotopes in nitrate, *Science*, 322, 730–732, doi:10.1126/science.1161910, 2008.

Obbard, R., Roscoe, H. K., Wolff, E. W., and Atkinson, H. M.: Frost flower surface area and chemistry as a function of salinity and temperature, *J. Geophys. Res*., 114, D20305, doi:10.1029/2009JD012481, 2009.

Oncley, S., Buhr, M., Lenschow, D., Davis, D., & Semmer, S.: Observations of summertime NO fluxes and boundary-layer height at the South Pole during ISCAT 2000 using scalar similarity. *Atmospheric Environment*, 38(32), 5389-5398, https://doi.org/10.1016/j.atmosenv.2004.05.053, 2004.

Oum, K. W., Lakin, M. J. and Finlayson-Pitts, B. J.: Bromine activation in the troposphere by the dark reaction of O_3 with seawater ice, *Geophys. Res. Lett*., 25(21), 3923–3926, doi:10.1029/1998GL900078, 953 1998.

https://doi.org/10.5194/egusphere-2022-696
Preprint. Discussion started: 18 October 2022

Parrella, J. P., D. J. Jacob, Q. Liang, Y. Zhang, L. J. Mickley, B. Miller, M. J. Evans, X. Yang, J. A. Pyle, N. Theys, and M. Van Roozendael: Tropospheric bromine chemistry: implications for present and pre-industrial ozone and mercury, *Atmos. Chem. Phys*., 12, 6723-6740, doi:10.5194/acp-12-6723-2012, 2012.Peterson P. K., Simpson, W. R,, Nghiem S. V.: Variability of Bromine Monoxide at Barrow, Alaska Over Four Halogen Activation (March-May) Seasons and at Two On-Ice Locations, *J Geophys Res – Atmos*., ISSN 2169897X. doi:https://doi.org/10.1002/2015JD024094, 2004.

Peterson, P. K., Hartwig, M., May, N. W., Schwartz, E., Rigor, I., Ermold, W., et al.: Snowpack measurements suggest role for multi-year sea ice regions in Arctic atmospheric bromine and chlorine chemistry, *Elementa: Science of the Anthropocene*, *7*. https://doi.org/10.1525/ elementa.352, 2019.

Piot, M.; von Glasow, R. The Potential Importance of Frost Flowers, Recycling on Snow, and Open Leads for Ozone Depletion Events. *Atmos. Chem. Phys*., 8, 2437−2467, 2008.

Piot, M.; von Glasow, R.: Modelling the Multiphase near-Surface Chemistry Related to Ozone Depletions in Polar Spring, *J. Atmos. Chem*. 64 (2−3), 77−105, 2009.

Pratt KA, Custard KD, Shepson PB, Douglas TA, Pöhler D, General S, Zielcke J, Simpson WR, Platt U, Tanner DJ, Gregory, Huey L, Carlsen M and Stirm BH.: Photochemical production of molecular bromine in Arctic surface snowpacks, *Nature Geoscience* 6(5): 351–356. ISSN 1752–0894, http://www.nature.com/doifinder/10.1038/ngeo1779. DOI: 10.1038/ngeo1779, 2013.

Rhodes, R. H., Yang, X., Wolff, E. W., McConnell, J. R., Frey, M. M.: Sea ice as a source of sea salt aerosol to Greenland ice cores: a model-based study. *Atmospheric Chemistry and Physics*, 17. 9417-9433. 10.5194/acp-17-9417-2017, 2017.

Rolph, G., Stein, A., and Stunder, B.: Real-time Environmental Applications and Display sYstem: READY, Environ. Modell. Softw., 95, 210–228, https://doi.org/10.1016/j.envsoft.2017.06.025, 2017.

Salawitch, R., Canty, T., Kurosu, T., Chance, K., Liang, Q., 19odelli, A., Pawson, S., Nielsen, J. E., Rodriguez, J. M., Bhartia, P. K., Liu, X., Huey, L. G., Liao, J., Stickel, R. E., Tanner, D.J., Dibb, J. E., Simpson, W. R., Donohoue, D., Weinheimer, A.,Flocke, F., Knapp, D., Montzka, D., Neuman, J. A., Nowak, J.B., Ryerson, T. B., Oltmans, S., Blake, D. R., Atlas, E. L., Kinni-son, D. E., Tilmes, S., Pan, L. L., Hendrick, F., Van Roozendael.,M., Kreher, K., Johnston, P. V., Gao, R. S., Johnson, B., Bui, T.P., Chen, G., Pierce, R. B., Crawford, J. H., and Jacob, D. J.: A new interpretation of total column BrO during Arctic spring, *Geophys. Res. Lett*., 37, L21805, doi:10.1029/2010GL043798, 2010.

Simpson, W. R., Alvarez-Aviles, L., Douglas, T. A., Sturm, M., and Domine, F.: Halogens in the coastal snow pack near Barrow, Alaska: Evidence for active bromine air-snow chemistry during springtime, *Geophys. Res. Lett*., 32, L04811, doi:10.1029/2004GL021748, 2005.

Simpson, W. R., et al.: Halogens and their role in polar boundary-layer ozone depletion, *Atmos. Chem. Phys.*, 7, 4375– 4418, 2007a.

Simpson, W. R., Carlson, D., Hönninger, G., Douglas, T. A., Sturm, M., Perovich, D., and Platt, U.: First-year sea-ice contact predicts bromine monoxide (BrO) levels at Barrow, Alaska better than potential frost flower contact, *Atmos. Chem. Phys*., 7, 621–627, https://doi.org/10.5194/acp-7-621-2007, 2007b.

Stein, A.F., Draxler, R.R, Rolph, G.D., Stunder, B.J.B., Cohen, M.D., and Ngan, F., NOAA's HYSPLIT atmospheric transport and dispersion 20odelling system, Bull. Amer. Meteor. Soc., 96, 2059-2077, http://dx.doi.org/10.1175/BAMS-D-14-00110.1, 2015.

Sturm, M. and Johnson, J. B.: Natural-convection in the sub-Arctic snow cover, *J. Geophys. Res.* -Solid Earth Planets, 96, 11657-11671, 1991.

Swanson, W. F., Holmes, C. D., Simpson, W. R., Confer, K., Marelle, L., Thomas, J. L., Jaeglé, L., Alexander, B., Zhai, S., Chen, Q., Wang, X., and Sherwen, T.: Comparison of model and ground observations finds snowpack and blowing snow both contribute to Arctic tropospheric reactive bromine, *Atmos. Chem. Phys. Discuss*. https://doi.org/10.5194/acp-2022-44, in review, 2022.

Stull, R. B., 1988: *An Introduction to Boundary Layer Meteorology.* Kluwer Academic, 666 pp.

Tarasick, D.W., and J.W Bottenheim, Surface ozone depletion episodes in the Arctic and Antarctic from historical ozonesonde records, *Atmos. Chem. Phys*., 2, 197-205, 2002.

Theys, N., Van Roozendael, M., Hendrick, F., Yang, X., De Smedt, I., Richter, A., Begoin, M., Errera, Q., Johnston, P. V., Kreher, K., and De Mazière, M.: Global observations of tropospheric BrO columns using GOME-2 satellite data, *Atmos. Chem. Phys*., 11, 1791-1811, doi:10.5194/acp-11-1791-2011, 2011.

Thomas, J. L., Stutz, J., Lefer, B., Huey, L. G., Toyota, K., Dibb, J. E., and von Glasow, R.: Modeling chemistry in and above snow at Summit, Greenland – Part 1: Model description and results, *Atmos. Chem. Phys*., 11, 4899–4914, https://doi.org/10.5194/acp-11-4899-2011, 2011.

Toyota, K.; McConnell, J. C.; Staebler, R. M.; Dastoor, A. P. Air−snowpack Exchange of Bromine, Ozone and Mercury in the Springtime Arctic Simulated by the 1-D Model PHANTAS Part 1: In-Snow Bromine Activation and Its Impact on Ozone. *Atmos. Chem. Phys*., 14 (8), 4101−4133, 2014.

Rolph, G., Stein, A., and Stunder, B., Real-time Environmental Applications and Display sYstem: READY. *Environmental Modelling & Software*, 95, 210-228, https://doi.org/10.1016/j.envsoft.2017.06.025, 2017.

Wagner, T. and Platt, U.: Observation of Tropospheric BrO from the GOME Satellite, Nature, 395, 486–490, 1998.

Wang, S., McNamara, S. M., Moore, C. W., Obrist, D., Steffen, A., Shepson, P. B., Staebler, R. M., Raso, A. R. W., Pratt, K. A.: Direct detection of atmospheric atomic bromine leading to mercury and ozone depletion, *Proceedings of the National Academy of Sciences,* 116 (29) 14479-14484; DOI: 10.1073/pnas.1900613116, 2019.

Warren, S. G., Rigor, I. G., Untersteiner, N., Radionov, V. F., Bryazgin, N. N., Aleksandrov, Y. I., & Colony, R.: Snow depth on Arctic sea ice, *Journal of Climate*, 12, 1814 -1829. https://doi.org/10.1175/1520-0442(1999)012<1814:SDOASI>2.0.CO;2, 1999.

Winton, V. H. L., Ming, A., Caillon, N., Hauge, L., Jones, A. E., Savarino, J., Yang, X., Frey, M. M.: Deposition, recycling and archival of nitrate stable isotopes between the air-snow interface: comparison between Dronning Maud Land and Dome C, Antarctica. *Atmospheric Chemistry and Physics*, 20. 5861-5885. 10.5194/acp-20-5861-2020, 2020.

https://doi.org/10.5194/egusphere-2022-696
Preprint. Discussion started: 18 October 2022

Yang, X., Cox, R. A., Warwick, N. J., Pyle, J. A., Carver, G. D., O'Connor, F. M., and Savage, N.H.: Tropospheric bromine chemistry and its impacts on ozone: A model study, *J. Geophys. Res.*, *110*, D23311, doi:10.1029/2005JD006244, 2005.

Yang, X., Pyle, J. A., and Cox, R. A.: Sea salt aerosol production and bromine release: Role of snow on sea ice, *Geophys. Res. Lett*., 35 (L16815), doi:10.1029/2008gl034536, 2008.

Yang, X., Pyle, J. A., Cox, R. A., Theys, N., and Van Roozendael, M.: Snow-sourced bromine and its implications for polar tropospheric ozone, Atm. Chem. Phys., 10, 7763-7773, doi:10.5194/acp-10-7763-2010, 2010.

Yang, X., Frey, M. M., Rhodes, R. H., Norris, S. J., Brooks, I. M., Anderson, P. S., Nishimura, K., Jones, A. E., and Wolff, E. W.: Sea salt aerosol production via sublimating wind-blown saline snow particles over sea ice: parameterizations and relevant microphysical mechanisms, *Atmos. Chem. Phys*., 19, 8407–8424, https://doi.org/10.5194/acp-19-8407-2019, 2019.

Yang, Xin, Blechschmidt, Anne-M., Bognar, Kristof, McClure-Begley, Audra, Morris, Sara, Petropavlovskikh, Irina, Richter, Andreas, Skov, Henrik, Strong, Kimberly, Tarasick, David W., Uttal, Taneil, Vestenius, Mika, Zhao, Xiaoyi.: Pan-Arctic surface ozone: modelling vs. measurements. *Atmospheric Chemistry and Physics*, 20. 31 pp. 10.5194/acp-20-15937-2020, 2020.

Zatko, M., Geng, L., Alexander, B., Sofen, E., and Klein, K.: The impact of snow nitrate photolysis on boundary layer chemistry and the recycling and redistribution of reactive nitrogen across Antarctica and Greenland in a global chemical transport model, *Atmos. Chem. Phys*., 16, 2819–2842, https://doi.org/10.5194/acp-16-2819-2016, 2016.

Zhou, X., Beine, H. J., Honrath, R. E., Fuentes, J. D., Simpson, W., Shepson, P. B., and Bottenheim, J.: Snowpack Photochemical Production as a Source for HONO in the Arctic Boundary Layer in Spring Time, *Geophys. Res. Lett*., 28 (21), 4087–4090, 2001.

Zhao, X., Strong, K., Adams, C., Schofield, R., Yang, X., Richter, A., Friess, U., Blechschmidt, A.-M., and Koo, J.-H.: A case study of a transported bromine explosion event in the Canadian high arctic, *J. Geophys. Res. -Atmos*., 121, 457–477, doi:10.1002/2015JD023711, 2016.

Zhao, X., Weaver, D., Bognar, K., Manney, G., Millán, L., Yang, X., Eloranta, E., Schneider, M., and Strong, K.: Cyclone-induced surface ozone and HDO depletion in the Arctic, *Atmos. Chem. Phys*., 17, 14955-14974, https://doi.org/10.5194/acp-17-14955-2017, 2017.

https://doi.org/10.5194/egusphere-2022-696
Preprint. Discussion started: 18 October 2022

Table 1. Mean and median snow salinities (psu) in tray samples at inland and sea ice sites. Surface snow (<0.5 cm) salinities at PEARL, Onshore and Sea ice sites are in two snow types: fluffy soft snow and aged hard snow.

	Snow types	Sample number	Year	Mean ± 1 standard deviation	Median
Tray samples	all	14	2019	0.0070±0.0088	0.0035
Inland samples[a]	all	211	2018, 2019	0.0290±0.1130	0.0115
Sea ice samples[b]	all	146	2018, 2019	0.2960±1.6400	0.0374
PEARL	fluffy soft	7	2018	0.0039±0.0029	0.0038
	aged hard	2	2018	0.0175±0.0046	0.0175
Onshore	fluffy soft	73	2018	0.0033±0.0027	0.0021
	aged hard	20	2018	0.0364±0.0112	0.0375
Sea ice	fluffy soft	44	2018	0.0105±0.0104	0.0057
	aged hard	17	2018	0.2372±0.3836	0.0896

[a] Inland data contain all salinity measurements for snow samples in the surface layers and columns collected at the Onshore, 0PAL/Creek, PEARL and airport sites. [b] Sea ice data contain all salinity measurements for samples in the surface layers and columns collected over sea ice (see Section 2.2).

https://doi.org/10.5194/egusphere-2022-696
Preprint. Discussion started: 18 October 2022

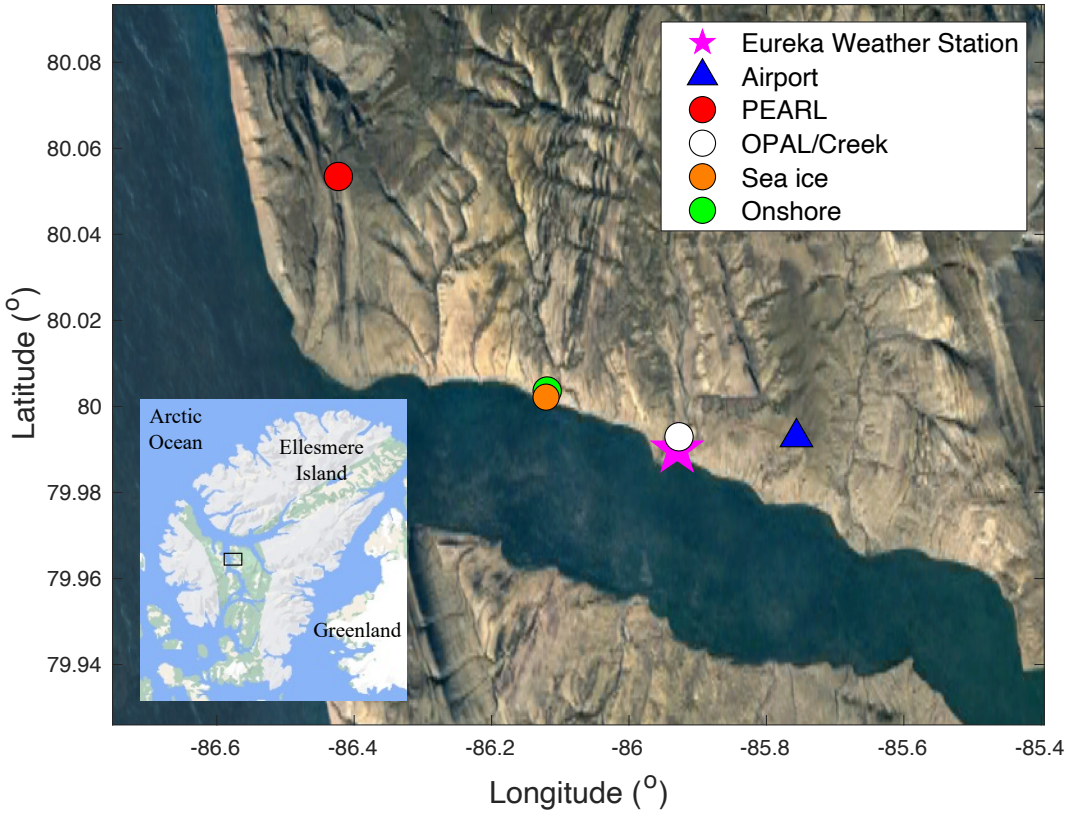

Figure 1. Local map with location of snow sampling sites marked by circles. The Eureka Weather Station (EWS) is marked by a star and the Eureka airport is marked by a triangle. The small inset box shows the location of the main map of Ellesmere Island, Canada. Images: © Google Earth/© Google Maps.

https://doi.org/10.5194/egusphere-2022-696
Preprint. Discussion started: 18 October 2022

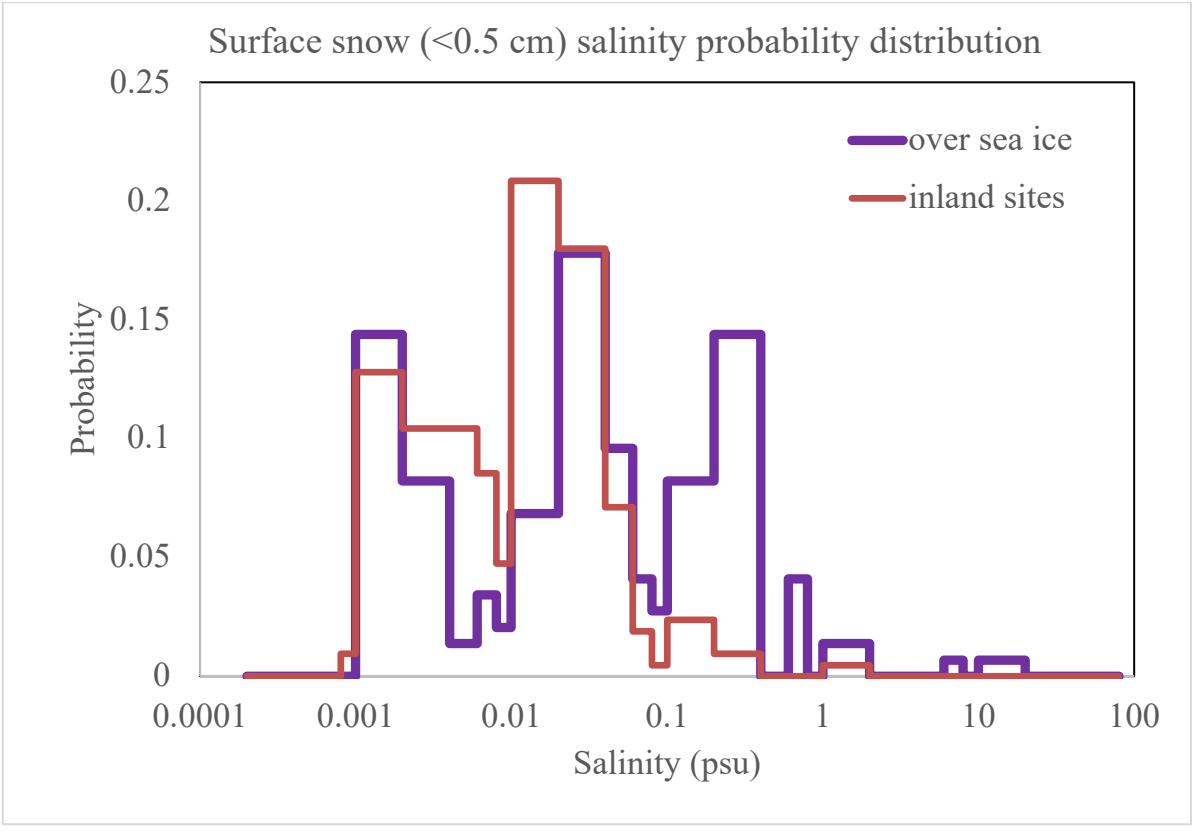

690

Figure 2. Eureka snow salinity probability distribution. The data include 2018 and 2019 snow sample measurements. The distribution over sea ice includes 146 snow samples, and the distribution at inland sites includes 211 snow samples (see Table 1).

https://doi.org/10.5194/egusphere-2022-696
Preprint. Discussion started: 18 October 2022

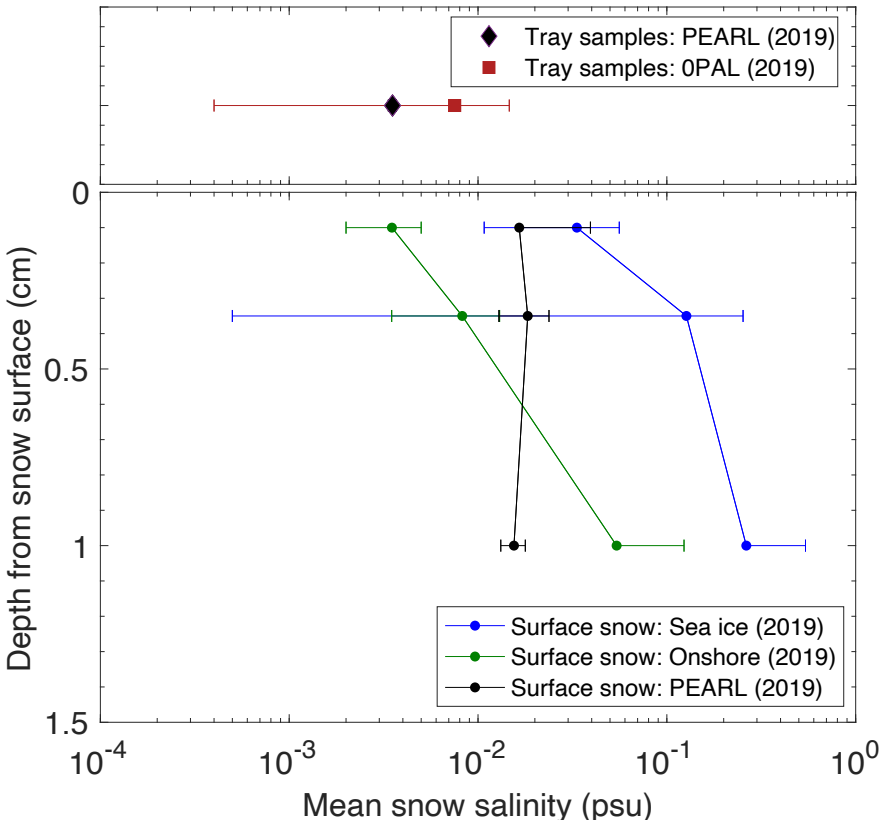

Figure 3. Mean snow salinity from the top 1.5 cm in three sub-layers: 0–0.2 cm, 0.2–0.5 cm, and 0.5–1.5 cm at the Sea ice, Onshore and PEARL sites (lower panel), and tray sample salinity at the 0PAL and PEARL sites (upper panel). The horizontal error bar represents one standard deviation. Note that tray samples at 0PAL were from a mounted tray outside the 0PAL building, approximately 1 m above the ground. Tray samples at PEARL were from a mounted tray (~1.5 m) on the roof of the PEARL Ridge Laboratory (~11 m above the ground).

https://doi.org/10.5194/egusphere-2022-696
Preprint. Discussion started: 18 October 2022

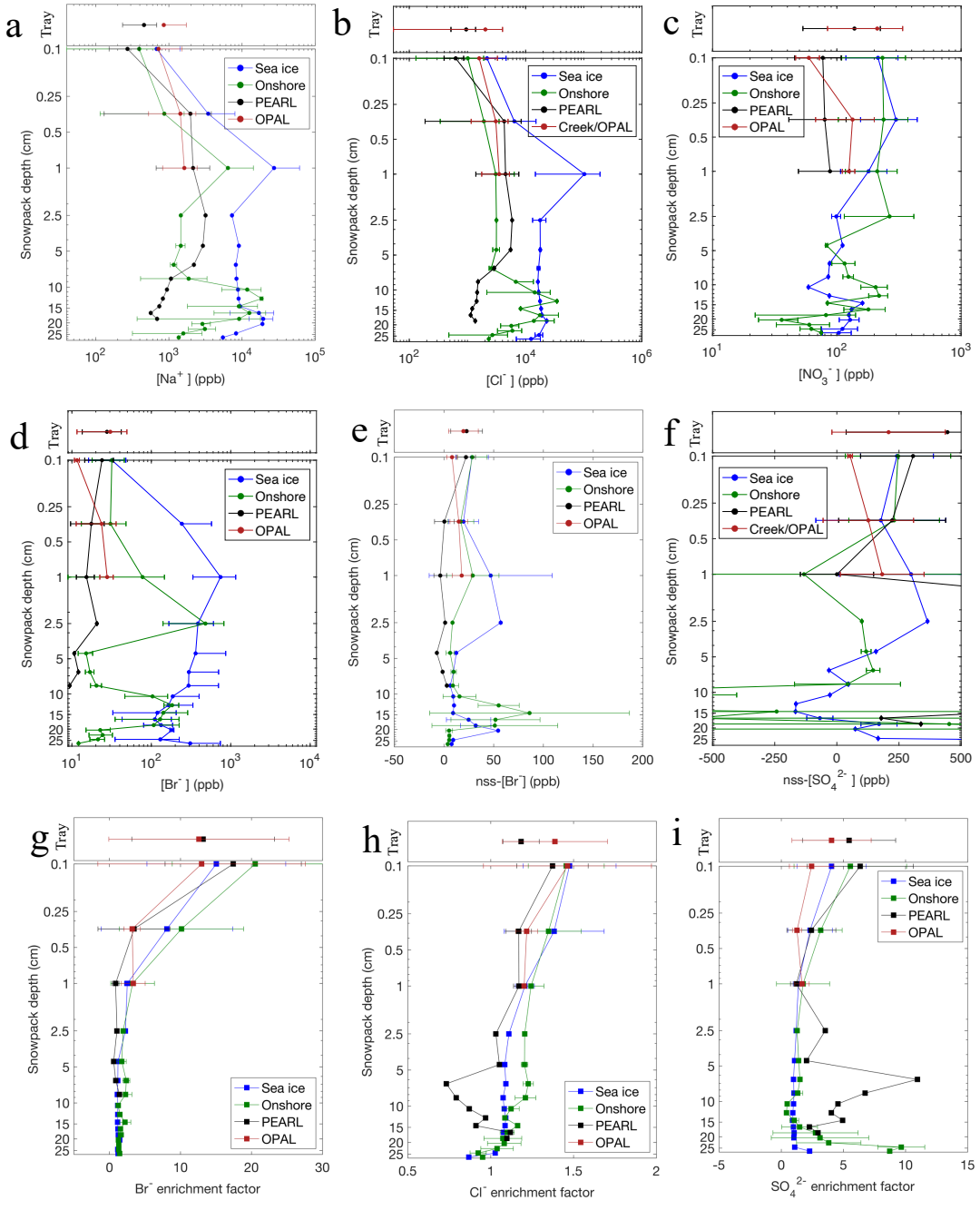

Figure 4. Vertical profiles of 2019 snow ions [Na^+] (a), [Cl-] (b), [NO_3^-] (c), [Br^-] (d), non-sea-salt (nss)[Br^-] (e), nss[SO_4^{2-}] (f) and enrichment factor of [Br^-] (g), [Cl^-] (h) and [SO_4^{2-}] (i) (see Section 3.2 for details).

705

https://doi.org/10.5194/egusphere-2022-696
Preprint. Discussion started: 18 October 2022

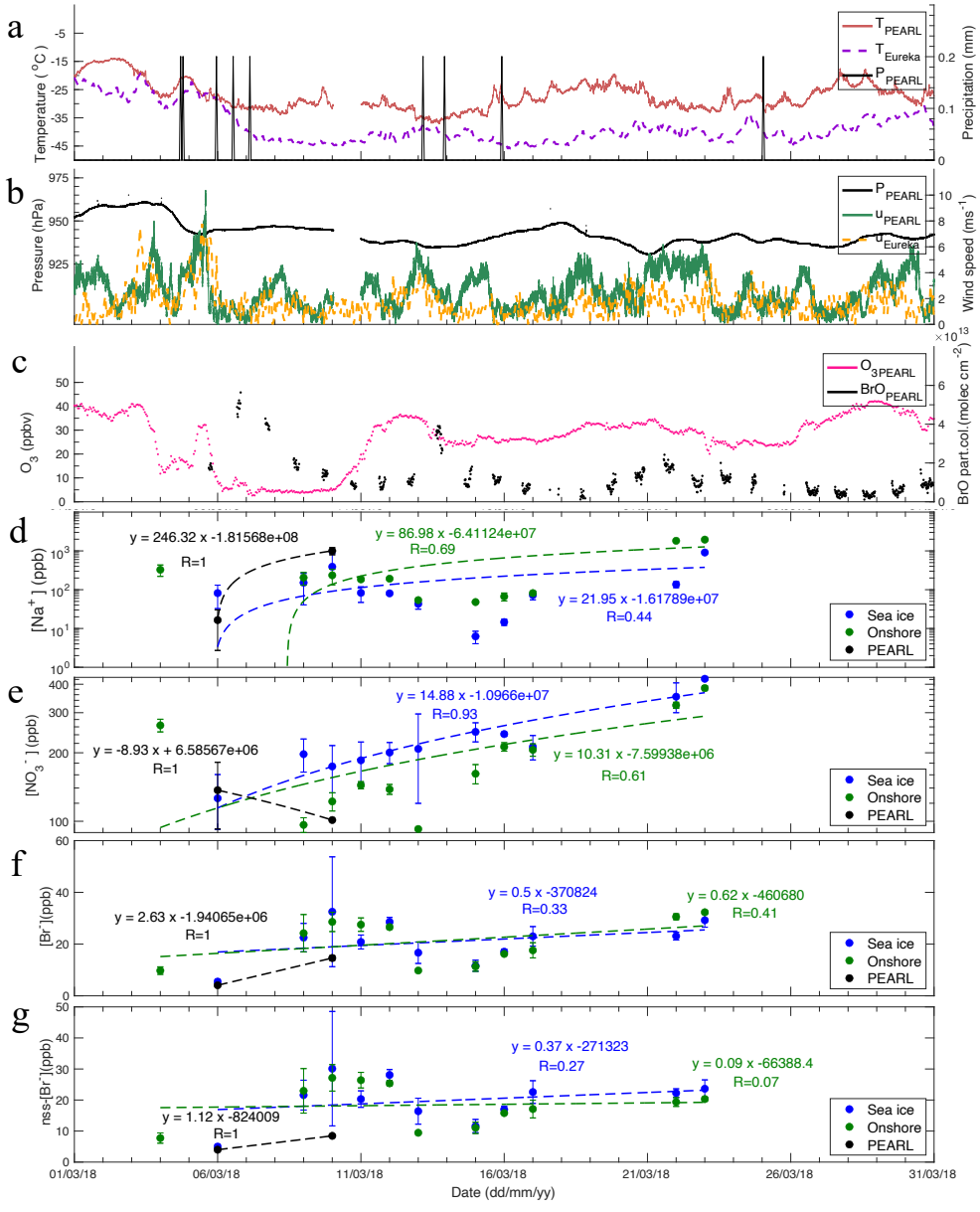

Figure 5. Time series of 2018 data. Meteorology data (temperature, precipitation, pressure and surface wind speed) from the Eureka Weather Station and PEARL Ridge Laboratory (a and b); Surface ozone at 0PAL and MAX-DOAS BrO (0-4 km) partial columns from the PEARL Ridge Laboratory (c); Top 0.5 cm snow [Na^+] (d), [NO_3^-](e), [Br^-] (f) and nss[Br^-] (g). Linear regression function (against time) and correlation coefficient R at each site are given.

https://doi.org/10.5194/egusphere-2022-696
Preprint. Discussion started: 18 October 2022

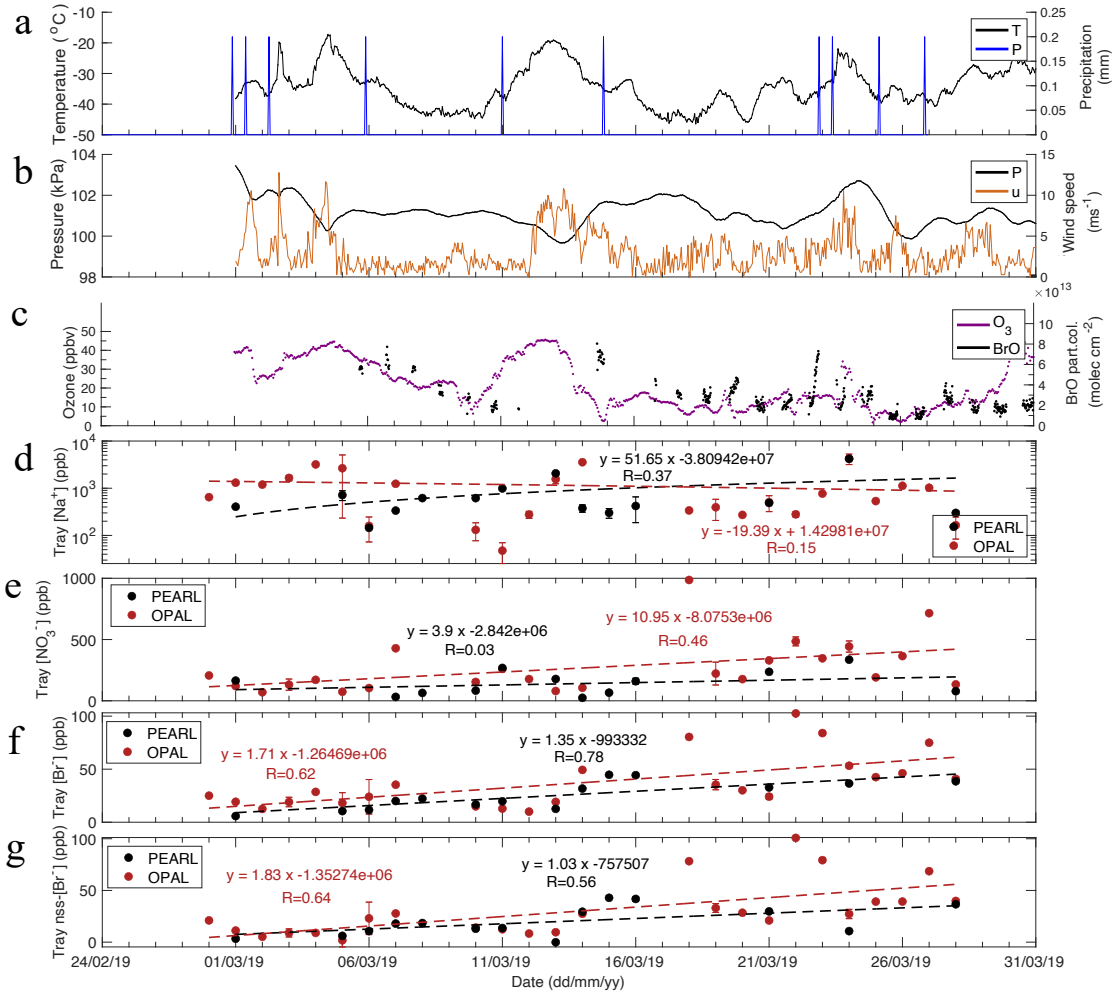

Figure 6. Time series of 2019 data. Meteorology data (temperature, precipitation, pressure and surface wind speed) from the Eureka Weather Station (a and b); Surface ozone at 0PAL and MAX-DOAS BrO partial columns from the PEARL Ridge Laboratory (c); Tray samples [Na^+] (d), [NO_3^-] (e), [Br^-] (f), and non-sea-salt (nss)[Br^-] (g). Linear regression function (against time) and correlation coefficient R at each site are given.

https://doi.org/10.5194/egusphere-2022-696
Preprint. Discussion started: 18 October 2022

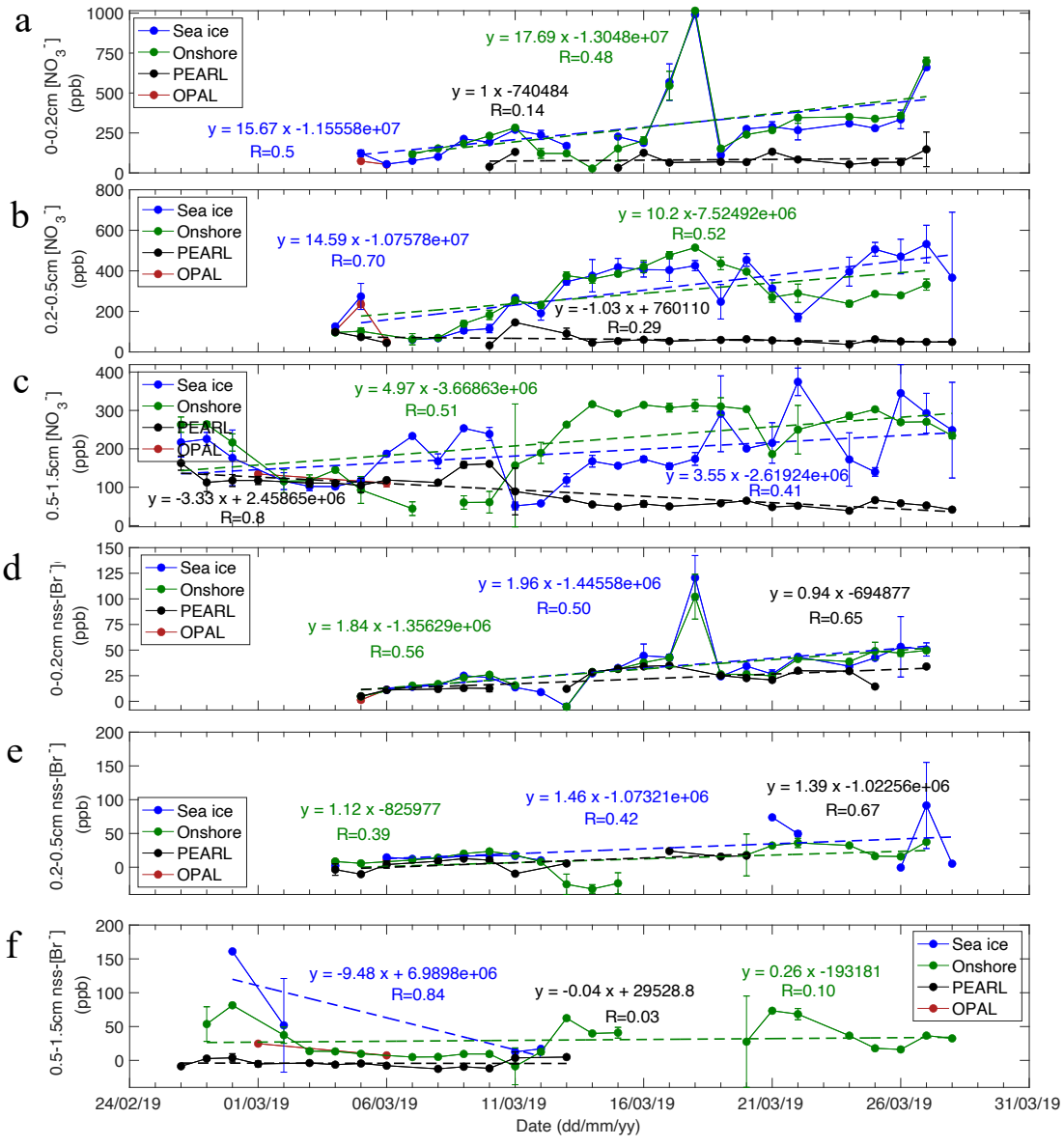

Figure 7. Time series of 2019 snow nitrate (a-c) and bromide (d-f) in three sub-layers: 0–0.2 cm, 0.2–0.5 cm, and 0.5–1.5 cm at four sampling sites: Sea ice, Onshore, PEARL and 0PAL. Linear regression function against time and correlation coefficient R are given.

https://doi.org/10.5194/egusphere-2022-696
Preprint. Discussion started: 18 October 2022

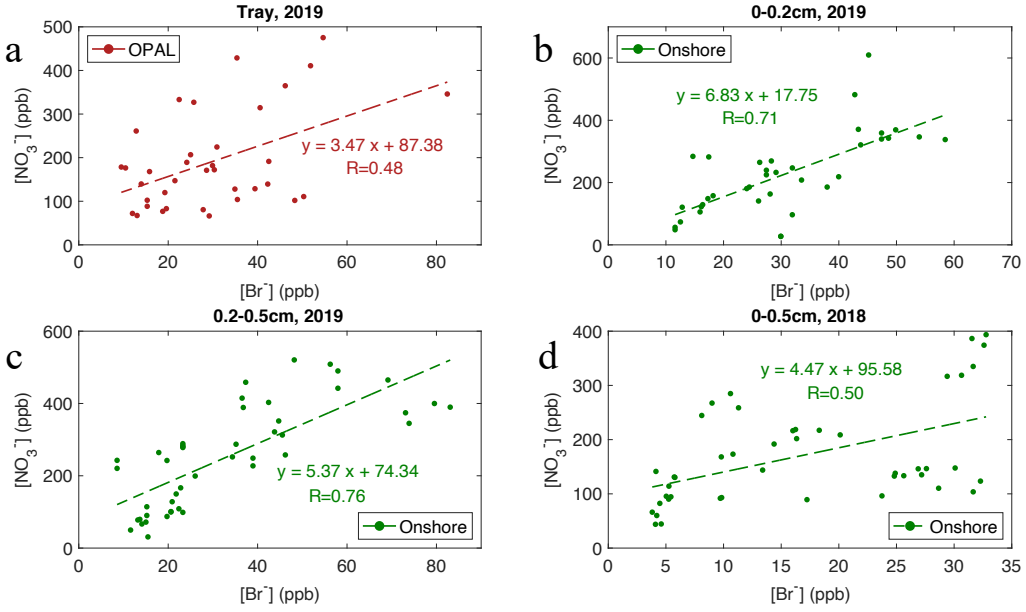

730 Figure 8. Scatter plot of surface snow nitrate versus bromide in (a) tray samples (2019), (b) 0–0.2 cm layer, (c) 0.2–0.5 cm layer (2019), and (d) 0–0.5 cm layer snow (2018). Linear regression and corresponding correlation coefficient R are given.